

# A Finite-Calibration Regime Map for LLM Judge Panels

Bin Zhu   Yanghui Rao\*  
 School of Computer Science and Engineering  
 Sun Yat-sen University

## Abstract

We study when LLM judge panels should be calibrated with low-dimensional stackers versus joint output tables under finite human-label budgets. Low-dimensional stackers have small estimation cost but miss interactions, whereas joint-table calibrators can represent interactions but pay for cell counts and unseen patterns. We cast this tradeoff as a finite-calibration regime map and instantiate it as *Finite-Calibration Panel Selection* (FCPS), a deployable validation selector over judge path, prefix size, and aggregator family with table and parametric estimation diagnostics. On RewardBench, LLMBench, SummEval, and Arena100K with a seven-judge pool including DeepSeek V4 Flash, scalar/reliability aggregation wins 16 of 20 real dataset-budget cells, indicating that current judge outputs are often additive or redundant. Controlled calibration-growth data show the complementary regime: additive labels remain scalar-favored, whereas a six-way interaction selects a larger joint table and its test MSE drops from 0.224 to 0.061 once unseen mass vanishes. Thus the practical question is not “how many judges?” but whether the next judge’s information is estimable under the available human labels.

## 1 Introduction

Automatic judges are widely used to evaluate language model outputs (Zheng et al., 2023; Liu et al., 2023; Zhu et al., 2023), and judge panels are often proposed to reduce single-judge bias (Verga et al., 2024). The finite-label catch is that more judges are information plus a calibration bill: the panel output must still be mapped to human labels. Adding one judge may reveal a useful interaction, or mostly split the calibration table into sparse cells.

We ask when a deployer should spend finite labels on a flexible joint table, and when the same labels are better spent on a lower-dimensional reliability or stacking model (Wolpert, 1992; Qian et al., 2026). The resulting object is an empirical finite-calibration regime map over task structure, panel size, aggregator family, and calibration budget.

For a target distribution  $P$ , ordered judge path  $\pi$ , prefix size  $K$ , output schema  $s$ , aggregator family  $\mathcal{A}$ , and labeled calibration budget  $n_M$ , let  $\hat{f}_{\pi,K,\mathcal{A}}$  be the predictor fitted from the calibration block. Its finite-sample risk is organized by the bookkeeping decomposition

$$\mathcal{R}(\hat{f}_{\pi,K,\mathcal{A}}) - \mathcal{R}^* \approx \text{Approx}(\pi, K, \mathcal{A}) + \text{Est}(\pi, K, \mathcal{A}, n_M) + \text{Sel}(\mathcal{C}, n_V), \quad (1)$$

where  $\mathcal{C}$  is the finite candidate menu and  $n_V$  is the validation size. The selection term is a property of the candidate set and validation sample, as in classical validation selection (Stone, 1974); the theorem below makes it explicit. The relevant decision object is

$$(\pi^*, K^*, \mathcal{A}^*) \in \arg \min_{(\pi,K,\mathcal{A}) \in \mathcal{C}} \mathcal{R}(\hat{f}_{\pi,K,\mathcal{A}}),$$

---

\*Corresponding author.

which selects a deployable panel/aggregator pair for the available label budget. For the joint-table family, the first two terms reduce to the familiar squared-loss identity  $\mathcal{R}_{\text{finite}} = \mathcal{R}_{\text{oracle}} + \mathcal{R}_{\text{cal}}$ : the Bayes table  $g^*(z) = \mathbb{E}[Y \mid Z_K = z]$  has no table-approximation error, and the finite calibration term includes smoothing bias, cell imbalance, and fallback error on unseen cells. Lower-dimensional stackers have smaller estimation cost but nonzero approximation error when judge interactions matter. Thus additive targets favor scalar stackers, while large non-additive interactions favor the joint table after labels cover the induced cell structure.

The experiments expose this tradeoff across real and controlled regimes. On four real benchmarks with a seven-judge pool including DeepSeek V4 Flash, validation-selected scalar aggregation beats validation-selected joint-table prefix calibration in 16 of 20 dataset–budget cells. The surprising lesson is that current real judge outputs often look additive or redundant enough that table flexibility is not worth its finite-label cost. Controlled calibration-growth regimes show the complementary case. In an additive regime, scalar models remain better as labels grow. In a six-way interaction regime, the selected table uses the interaction-bearing prefix and improves sharply as unseen cells disappear. The same finite-calibration theory explains both outcomes.

The practical output is FCPS: reserve calibration and validation labels, generate judge paths, train candidate aggregators for each prefix, select  $(\hat{\pi}, \hat{K}, \hat{A})$  by validation risk, and report effective support, exact cell pressure, and unseen rate. The contribution is the finite-calibration regime map, deployable selector, and diagnostics that connect the selected panel to finite-support pressure. In this view, panel complexity must be earned by calibration evidence.

**Contribution.** Our central contribution is a finite-calibration regime map for deploying LLM judge panels: jointly select the judge prefix and aggregation family under the available human-label budget. This has three components.

1. **Regime theory.** We define the deployable object as  $(K, \mathcal{A})$ , decompose finite risk into approximation, estimation, and selection terms, and derive table/stacking comparisons that describe when a flexible table can beat a low-dimensional aggregator.
2. **Deployable selection with diagnostics.** We instantiate the theory as FCPS, a validation selector over paths, prefixes, and aggregator families, and report exact cell pressure, effective support, and unseen mass so the selected regime is interpretable rather than a black-box ensemble choice.
3. **Two-sided empirical evidence.** Real benchmarks show the additive/redundant side of the map, where scalar aggregation often wins; controlled calibration-growth regimes show the interaction side, where the joint table improves as labels remove sparse-cell pressure.

## 2 Related Work

**LLM-as-a-judge evaluation.** Large language models are now widely used as automatic evaluators for open-ended generation. MT-Bench and Chatbot Arena popularized LLM judges for pairwise and multi-turn evaluation (Zheng et al., 2023), while G-Eval showed that prompted GPT-style evaluators can align strongly with human judgments for NLG tasks (Liu et al., 2023). JudgeLM studies fine-tuning scalable open-source judges and documents judge biases such as position, knowledge, and format effects (Zhu et al., 2023); agreeableness-bias work studies another axis of judge reliability (Jain et al., 2025). Benchmarks such as LLMBench, RewardBench, and SummEval stress different parts of the evaluator problem: instruction-following meta-evaluation, reward/preference modeling, and summarization quality assessment (Zeng et al., 2024; Lambert et al., 2024; Fabbri et al., 2021). Deterministic learned metrics have also been proposed as alternatives to costly and stochastic LLM judges (Alam et al., 2026). This paper uses existing judge outputs

and benchmarks not to propose another evaluator benchmark, but to study how a finite calibration budget should determine the number of judges and aggregator family used from a fixed pool.

**Judge panels and finite-budget judge reliability.** Recent work has argued that panels or “juries” of diverse LLM judges can outperform a single large judge and reduce single-model bias (Verga et al., 2024). Our results refine this intuition: panels are useful, but the deployed panel size should still be selected under the available calibration budget. Concurrent work on label-efficient estimation from noisy LLM judges argues that a calibrated full panel can outperform accuracy-based judge curation when the full joint signal is learnable (Li, 2026). This is complementary to our framing: their oracle-style message emphasizes that additional judge signals need not hurt with enough calibration, while our finite-table diagnostics study when the induced pattern table becomes too sparse for a limited calibration set. Other recent multi-judge approaches model repeated samples or judge heterogeneity more explicitly: distribution-calibrated inference-time judging uses a Bradley–Terry–Davidson aggregation of repeated thinking-judge samples (Dadkhahi et al., 2025), BT- $\sigma$  estimates judge reliability in an LLM-as-a-jury Bradley–Terry model without human calibration labels (Qian et al., 2026), and heterogeneous judge-aware ranking separates consensus ranking, judge sensitivity, and residual disagreement (Yu et al., 2026). We include a representative Dawid–Skene/BT-style heterogeneous jury baseline in Appendix C as a point of comparison within this broader family. Selective conformal pairwise judging methods such as SCOPE provide finite-sample risk control through abstention and uncertainty calibration (Badshah et al., 2026); our protocol instead studies which judge prefix and aggregator to deploy when the system must output calibrated predictions for all examples.

**Calibration and finite-sample reliability.** Calibration has a long statistical history (Dawid, 1982) and is central to turning model scores into reliable probabilities. Practical post-hoc calibration methods such as Platt scaling and temperature scaling estimate a calibration map from held-out labels (Platt, 1999; Guo et al., 2017). Practical LLM-judge improvement studies also consider drop-in prompting, ensembling, calibration context, and adaptive escalation techniques (Lail and Markham, 2026). Our setting differs because the object to be calibrated is not a single scalar score, but a joint judge-output pattern table whose support grows with the panel size. The finite-table bound in Proposition 1 makes this dependence explicit and motivates the empirical diagnostics based on entropy-effective support and unseen pattern rate. Other uncertainty-aware judge calibration methods estimate confidence from hidden-state probes (Radharapu et al., 2025) or return conformal prediction intervals for judge scores (Sheng et al., 2025). Noise-response calibration studies reliability under controlled perturbations and distribution shift (Khomiakov and Frelsen, 2026). Recent work also calibrates cheap judge surrogates to oracles, gives valid inference with imperfect judges, or uses multidimensional rubric calibration (Landesberg and Narayan, 2025; Feng et al., 2026; Hashemi et al., 2024). These methods calibrate a fixed judge, metric, or rubric representation; our focus is which panel prefix and aggregation family can be calibrated under a fixed label budget.

**Model selection and ensembles.** Validation-based model selection is standard under finite data (Stone, 1974), and stacking combines predictors to improve accuracy (Wolpert, 1992). Judge-panel selection adds a calibration constraint: adding a judge changes the joint-pattern alphabet estimated from human labels. The decision is therefore whether the next judge’s information gain is worth the extra calibration complexity.

### 3 Finite-Calibration Panel Selection

#### 3.1 Decision Object

A deployment decision consists of a judge path  $\pi$ , a prefix size  $K$ , and an aggregator family  $\mathcal{A}$ . The family  $\mathcal{A}$  specifies how labeled calibration examples are used to map the first  $K$  judge outputs to a calibrated prediction. In this paper, the main nonparametric family is the joint table in Eq. (12); the main low-dimensional alternatives are mean aggregation with isotonic calibration, ridge stacking with isotonic calibration, and logistic stacking, following standard post-hoc calibration and stacking ideas (Platt, 1999; Guo et al., 2017; Wolpert, 1992).

The finite-calibration decision is

$$(\hat{\pi}, \hat{K}, \hat{\mathcal{A}}) \in \arg \min_{\pi \in \Pi, K \in \{1, \dots, m\}, \mathcal{A} \in \mathfrak{A}} \widehat{\mathcal{R}}_{\text{val}}(\hat{f}_{\pi, K, \mathcal{A}}). \quad (2)$$

The original path/prefix selector is the special case where  $\mathfrak{A} = \{\text{joint table}\}$ . The scalar aggregation base-lines and the controlled regime experiment use the same validation principle while varying  $\mathcal{A}$ . We call this deployable validation-over-candidates procedure *Finite-Calibration Panel Selection* (FCPS), a finite-candidate validation selector (Stone, 1974). The method is intentionally simple: its novelty is not the validation argmin itself, but the finite-calibration candidate space over paths, prefix sizes, and aggregation families together with the diagnostics used to interpret the selected regime.

**Theorem 1** (Finite validation selection). *Let  $\mathcal{C}$  be a finite set of candidate deployment choices  $(\pi, K, \mathcal{A})$ . For each  $c \in \mathcal{C}$ , let  $\hat{f}_c$  be the predictor produced from the selection and calibration blocks, and let  $\hat{c} = \arg \min_{c \in \mathcal{C}} \widehat{\mathcal{R}}_{\text{val}}(\hat{f}_c)$  be the validation selector. If the loss is bounded in  $[0, 1]$ , then conditional on the fitted candidate predictors, with probability at least  $1 - \delta$  over the validation block,*

$$\mathcal{R}(\hat{f}_{\hat{c}}) \leq \min_{c \in \mathcal{C}} \mathcal{R}(\hat{f}_c) + 2\sqrt{\frac{\log(2|\mathcal{C}|/\delta)}{2n_V}}. \quad (3)$$

*Proof.* See Appendix B. □

Theorem 1 is the finite-menu analogue of standard validation/cross-validation selection with bounded-loss concentration (Stone, 1974; Hoeffding, 1963) and isolates the selection term in Eq. (1). Expanding the candidate set to include more paths, prefixes, and aggregator families increases the validation penalty only logarithmically in the number of fitted candidates, but it still requires a held-out validation block that is separate from the final test block.

#### 3.2 Judge Paths and Prefixes

Let  $\mathcal{J} = \{j_1, \dots, j_m\}$  be a pool of judges. A path rule produces an ordering  $\pi$  of this pool. For each prefix size  $K$ , the deployed panel is the first  $K$  judges along the path. The path rule therefore determines which joint pattern table is exposed as  $K$  grows.

We consider three path rules. The *information-first path* orders judges by single-judge oracle performance on the selection block and should be read as the strong path baseline. The *random path* is a null baseline. The *complexity-penalized path* is a candidate heuristic motivated by Eq. (1). Let  $A$  be the current prefix, let  $\widehat{\mathcal{R}}_{\text{sel}}^*(A)$  be the empirical oracle risk obtained by grouping the selection block by the joint pattern of judges in  $A$ , and let  $H_{\text{sel}}(A)$  be the entropy-effective support of those selection-block patterns, defined by the same natural-log entropy formula as  $H_K$  below but on the selection block. Starting from the empty

prefix, the next judge is

$$j^* \in \arg \max_{j \notin A} \left[ \widehat{\mathcal{R}}_{\text{sel}}^*(A) - \widehat{\mathcal{R}}_{\text{sel}}^*(A \cup \{j\}) - \lambda \frac{(H_{\text{sel}}(A \cup \{j\}) - H_{\text{sel}}(A))_+}{n_M} \right]. \quad (4)$$

All experiments use  $\lambda = 1$ ; the denominator is the planned calibration budget  $n_M$  for the later fitted table. This fixed normalization keeps the path heuristic independent of validation and test outcomes. Thus the path rule uses the selection block only; the calibration and validation blocks are reserved for table fitting and prefix selection. The empirical selector then compares the candidate paths through the same validation envelope.

### 3.3 A Finite-Table Calibration Bound

We now make the calibration-complexity term in Eq. (1) more explicit. The argument is a finite partition-estimator calculation (Györfi et al., 2002): it abstracts away the judge identities and focuses on the induced output-pattern table.

For a fixed  $(P, K, \pi, s)$ , let  $Z_K$  be the joint output pattern of the first  $K$  judges along path  $\pi$ , and let  $\mathcal{Z}_K$  be its pattern space. A table calibrator estimates a conditional prediction rule  $g^*(z) = \mathbb{E}[Y \mid Z_K = z]$  from  $n_M$  labeled calibration examples. Let  $N_z$  be the number of calibration examples in cell  $z$ , and let  $\widehat{g}(z)$  be the empirical cell estimate with bounded loss in  $[0, 1]$ .

**Proposition 1** (Joint-table estimation with unseen mass). *Fix a prefix  $K$ , path  $\pi$ , and schema  $s$ . Let  $\widehat{\mathcal{Z}}_K = \{z : N_z > 0\}$  be the occupied calibration support,  $S_K = |\widehat{\mathcal{Z}}_K|$ ,  $p_z = P(Z_K = z)$ , and  $u_K = P(Z_K \notin \widehat{\mathcal{Z}}_K)$  be the test-time unseen mass. Suppose  $Y \in [0, 1]$ , predictions are clipped to  $[0, 1]$ , and the table uses the smoothed estimate*

$$\widetilde{g}(z) = \frac{N_z \bar{Y}_z + \alpha \bar{y}_{\text{cal}}}{N_z + \alpha}$$

*on occupied cells and the fallback  $\bar{y}_{\text{cal}}$  on unseen cells. With probability at least  $1 - \delta$ , uniformly over occupied cells,*

$$|\bar{Y}_z - g^*(z)| \leq \sqrt{\frac{\log(2S_K/\delta)}{2N_z}}. \quad (5)$$

*Consequently, the squared-loss excess risk of the deployed table relative to the Bayes table satisfies*

$$\mathcal{R}(\widetilde{g}) - \mathcal{R}(g^*) \leq 2 \sum_{z \in \widehat{\mathcal{Z}}_K} p_z \frac{\log(2S_K/\delta)}{2N_z} + 2 \sum_{z \in \widehat{\mathcal{Z}}_K} p_z \left( \frac{\alpha}{N_z + \alpha} \right)^2 + u_K. \quad (6)$$

*Proof.* See Appendix B. □

**Remark 1.** *The experiments use entropy-effective support rather than raw occupied support  $S_K$ , because the pattern table can be highly imbalanced. With calibration counts  $N_z$ ,  $\widehat{p}_z = N_z/n_M$  on  $\widehat{\mathcal{Z}}_K = \{z : N_z > 0\}$ , and natural logarithms, define  $H_K^{\text{eff}} = \exp(-\sum_{z \in \widehat{\mathcal{Z}}_K} \widehat{p}_z \log \widehat{p}_z)$ ; for brevity write  $H_K = H_K^{\text{eff}}$ . This is an empirical effective number of occupied calibration patterns. The diagnostic  $H_K/n_M$  is a practical pressure proxy; the plug-in cell-pressure quantity below is the closer observable counterpart of the bound. Proposition 1 gives a worst-case bounded-loss control by upper bounding unseen-cell contribution by  $u_K$ .*

The literal table pressure in Eq. (6) is

$$V_K(D_M) = \sum_{z: N_z > 0} p_z N_z^{-1} + P(Z_K \notin \widehat{\mathcal{Z}}_K), \quad (7)$$

up to logarithmic, smoothing, and bounded-loss constants. In the experiments we reconstruct the calibration cell counts and report the plug-in diagnostic  $\widehat{V}_K^{\text{cell}} = \sum_{z: N_z > 0} \widehat{p}_{\text{test}}(z)/N_z + \widehat{u}_K$ , where  $\widehat{p}_{\text{test}}$  and  $\widehat{u}_K$  are computed on the held-out test block. This is still empirical because it replaces the population cell masses  $p_z$  with held-out frequencies, but it is the closest observable counterpart of Eq. (7). We also report  $\widetilde{V}_K = H_K/n_M + \widehat{u}_K$  as a cheaper proxy. The following simplified calculation makes this relationship explicit and gives a concrete regime boundary.

**Proposition 2** (Balanced-support table scale). *Fix  $K, \pi, s$ , and suppose the population support of  $Z_K$  has size  $M_K$ . Assume approximate balance: for a constant  $c \geq 1$ ,*

$$\frac{1}{cM_K} \leq p_z \leq \frac{c}{M_K} \quad \text{for every support cell } z.$$

*If  $n_M \geq CcM_K \log(M_K/\delta)$ , then with probability at least  $1 - \delta$ , all population cells are observed and the joint-table excess risk in Proposition 1 is at most*

$$\mathcal{R}(\widetilde{g}) - \mathcal{R}(g^*) \leq C'c^2 \frac{M_K \log(M_K/\delta)}{n_M} + O\left(\frac{\alpha^2 M_K}{n_M^2}\right). \quad (8)$$

*Conversely, for Bernoulli targets with conditional variance bounded below by  $\sigma^2 > 0$  on each cell, estimating an unrestricted table over  $M_K$  cells has minimax expected squared excess risk at least*

$$\Omega\left(\frac{\sigma^2 M_K}{n_M}\right)$$

*in this balanced-support regime.*

*Proof sketch.* See Appendix B. □

**Corollary 1** (Approximation–estimation boundary). *For a scalar aggregator family  $\mathcal{A}$ , define its approximation gap relative to the unrestricted table Bayes rule as*

$$\Delta_K(\mathcal{A}) = \inf_{f \in \mathcal{A}} \mathcal{R}(f) - \mathcal{R}(g_K^*),$$

*where  $g_K^*(z) = \mathbb{E}[Y \mid Z_K = z]$ . Let  $E_{\text{tab}}(K, n_M)$  denote the table estimation pressure, e.g. the right-hand side of Eq. (8), and let  $E_{\text{scal}}(K, \mathcal{A}, n_M)$  denote the scalar-family estimation pressure, e.g. Eq. (10). Up to constants and validation-selection penalties, the joint table is preferable when*

$$\Delta_K(\mathcal{A}) \gtrsim E_{\text{tab}}(K, n_M) - E_{\text{scal}}(K, \mathcal{A}, n_M), \quad (9)$$

*whereas the scalar family is preferable when the inequality is reversed. Thus low-dimensional regimes have small  $\Delta_K(\mathcal{A})$  and favor scalar aggregation; interaction-heavy regimes have large  $\Delta_K(\mathcal{A})$  and favor the table once  $n_M$  is large enough to make  $E_{\text{tab}}$  affordable.*

### 3.4 Aggregator Complexity Regimes

The table bound identifies the cost of one high-flexibility family. Other families trade this estimation cost for structural approximation bias. A ridge or logistic stacker with  $K$  scalar judge features has parameter dimension  $O(K)$ , so its generic bounded-loss estimation pressure is closer to a parametric  $O(\sqrt{K/n_M})$  uniform-convergence scale, with faster  $O(K/n_M)$ -type rates possible only under stronger squared-loss or well-specified assumptions. In either case the dependence is polynomial in  $K$ , unlike the joint-table cell pressure from Proposition 2 when the effective support is  $M_K$ . The price is that a linear stacker cannot represent arbitrary interactions among judge outputs.

Aggregator family	Approximation behavior	Estimation pressure
Mean/vote + calibration	Strong additive restriction	one scalar calibration map
One-coin reliability	Conditional-independence reliability	$O(K)$ reliability parameters
Ridge/logistic stacking	Additive judge effects	$O(K)$ scalar features
Pairwise stacker	Low-order interactions	$O(K^2)$ interaction features
Joint table	Arbitrary categorical interactions	cell pressure $V_K(D_M)$

This is the main theoretical reconciliation with scalar aggregation baselines. If the true judge signal is mostly additive or redundant, stacking should often beat a joint table under finite labels. If the signal contains important output-pattern interactions, the joint table can be better once the calibration budget is large enough to estimate the relevant cells. The empirical baselines below instantiate this complexity ladder only approximately: isotonic post-calibration, one-coin reliability, and pairwise feature expansions are practical comparator families, while the formal parametric statement below covers the simpler bounded linear/Lipschitz class using standard Rademacher-complexity control (Bartlett and Mendelson, 2002).

**Proposition 3** (Parametric stacking estimation scale). *Let  $x \in [0, 1]^K$  be the vector of scalarized judge outputs for a  $K$ -judge prefix, and let  $\mathcal{F}_{K,B} = \{x \mapsto \phi(w^\top x + b) : \|w\|_2 \leq B, |b| \leq B\}$ , where  $\phi$  is a 1-Lipschitz clipping or sigmoid map. For any  $L$ -Lipschitz loss bounded in  $[0, 1]$ , empirical risk minimization over  $\mathcal{F}_{K,B}$  satisfies, with probability at least  $1 - \delta$ ,*

$$\mathcal{R}(\hat{f}) \leq \inf_{f \in \mathcal{F}_{K,B}} \mathcal{R}(f) + O\left(LB\sqrt{\frac{K}{n_M}} + \sqrt{\frac{\log(1/\delta)}{n_M}}\right). \quad (10)$$

*Proof sketch.* See Appendix B. □

Proposition 3 shows how stacking replaces the joint-table support term in Eq. (6) with a lower-dimensional estimation term, while paying the approximation term  $\inf_{f \in \mathcal{F}_{K,B}} \mathcal{R}(f) - \mathcal{R}(g^*)$  whenever the Bayes rule depends on interactions that the additive stacker cannot express. The formal statement covers a bounded linear/Lipschitz class; isotonic calibration, one-coin reliability, and pairwise expansions enter the experiments as natural deployable aggregators. Thus Corollary 1 supplies a complexity template for the scalar menu, with squared loss on  $[0, 1]$  changing constants.

### 3.5 FCPS Protocol

Given a calibration budget  $n_M$ , we split labeled data into selection, calibration, validation, and test blocks. For each candidate path rule and prefix size  $K$ , we fit a calibration map on the calibration block and evaluate finite risk on the validation block. For the joint-table experiments, the selected prefix is

$$(\hat{\pi}, \hat{K}) \in \arg \min_{\pi \in \Pi, K \in \{1, \dots, m\}} \hat{\mathcal{R}}_{\text{val}}(\hat{f}_{\pi, K, \text{tab}}). \quad (11)$$

This is Eq. (2) restricted to  $\mathfrak{A} = \{\text{joint table}\}$ . The test block is used only to evaluate the selected decision and to study diagnostic quantities such as unseen pattern rate.

This framing separates FCPS from any single path generator or aggregator. In the real-data experiments, joint-table path/prefix selection and scalar-family selection use the same calibration/validation/test separation, so Tables 3–11 compare families under a common validation-selection protocol rather than one path generator.

In the present implementation, the calibration map is a finite pattern-table estimator. Each observed joint judge-output pattern is mapped to its empirical calibration target on the calibration block, smoothed toward

the calibration marginal with  $\alpha = 0.5$ :

$$\widehat{g}(z) = \frac{\sum_{i:Z_i=z} y_i + \alpha \bar{y}_{\text{cal}}}{N_z + \alpha}. \quad (12)$$

Patterns not observed during calibration are assigned the fallback prediction  $\bar{y}_{\text{cal}}$ . We report the unseen pattern rate because this fallback is exactly where finite calibration pressure becomes visible. Risk is the mean squared calibration error,  $\frac{1}{|D|} \sum_{i \in D} (y_i - \widehat{g}(Z_i))^2$ , on the validation or test block. All path construction and prefix selection use only the selection/calibration/validation blocks; the test block is held out for final evaluation and diagnostics. With its global fallback, this joint table is a nonparametric endpoint; hierarchical backoff, Bayesian smoothing, and residual shrinkage are middle families between scalar stackers and a fully unrestricted table (Dawid, 1982; Wolpert, 1992).

**Algorithmic protocol.** The procedure used in our experiments is:

**FCPS: finite-calibration panel selection**

**Input:** labeled examples, judge pool  $\mathcal{J}$ , path rules  $\Pi$ , aggregator families  $\mathfrak{A}$ , calibration budget  $n_M$ , schema  $s$ , prefix set  $\{1, \dots, m\}$ .

**For each split:**

1. Partition labeled examples into selection, calibration, validation, and test blocks.
2. Generate candidate paths  $\pi \in \Pi$  using only the selection block.
3. For each path  $\pi$ , prefix size  $K$ , and aggregator family  $\mathcal{A}$ , fit the aggregator on the calibration block.
4. Evaluate validation risk  $\widehat{\mathcal{R}}_{\text{val}}(\widehat{f}_{\pi,K,\mathcal{A}})$ .
5. Select  $(\widehat{\pi}, \widehat{K}, \widehat{\mathcal{A}})$  by Eq. (2). For the joint-table-only experiments, this reduces to Eq. (11).
6. Report test risk and diagnostics for the selected decision.

**Output:** selected path, prefix size, aggregator family, test risk, entropy-effective support  $H_K$ , exact cell pressure, and unseen pattern rate.

**Hybrid shrinkage extension.** The theory also suggests a natural fallback aggregator that is more structured than a pure table but less biased than a scalar stacker. Given a scalar predictor  $f_{\text{scal}}(x)$  and a residual table  $\widehat{r}(z)$  fit on  $Y - f_{\text{scal}}(X)$ , deploy

$$f_{\text{hyb}}(x, z) = f_{\text{scal}}(x) + \frac{N_z}{N_z + \tau} \widehat{r}(z), \quad (13)$$

with the shrinkage strength  $\tau$  selected on validation data. This count-weighted hybrid directly encodes the table-estimation pressure: well-observed cells can add an interaction correction, while sparse or unseen cells fall back to the scalar model. Appendix C reports this prototype diagnostic; the main comparison uses the pre-specified table/scalar menu, where the strongest scalar selector remains the most stable real-data comparator.

### 3.6 Complexity Diagnostics

The calibration-complexity term is operationalized through effective support and unseen pattern diagnostics. For a prefix of size  $K$ ,  $H_K$  denotes the entropy-effective occupied support from the natural-log definition

Dataset	calibration budgets $n_M$	select/validation/test	schema
RewardBench	50, 100, 200, 400, 800	300 / 300 / 600	pairwise
LLMBar	20, 50, 100, 200, 300	100 / 100 / 200	pairwise
SummEval	32, 64, 128, 256, 512, 800	192 / 192 / 384	scalar
Arena100K	50, 100, 200, 400	200 / 200 / 400	pairwise

Table 1: Experimental protocol. Each row uses 30 grouped splits, smoothing  $\alpha = 0.5$ , and prefix sizes  $K \in \{1, \dots, 7\}$ .

above, and  $Q_K$  denotes the nominal pattern alphabet size. We use  $H_K/n_M$  as a practical proxy for finite-budget pattern pressure and report  $\tilde{V}_K = H_K/n_M + \hat{u}_K$  when we want a single observable diagnostic for the table pressure in Eq. (7). We also measure the test-time unseen pattern rate, the fraction of test patterns not observed in the calibration block. These quantities are not themselves guaranteed excess-risk terms; they audit regimes in which the literal table-bound quantities, especially small cell counts and unseen mass, are likely to matter.

## 4 Experiments

We evaluate FCPS on RewardBench, LLMBar, SummEval, and Arena100K (Lambert et al., 2024; Zeng et al., 2024; Fabbri et al., 2021; Tang et al., 2025; Chiang et al., 2024) with a fixed seven-judge pool: Qwen2.5-7B, Llama-3.1-8B, Mistral-7B, Prometheus-7B, Gemma-3-12B, Selene-8B, and DeepSeek V4 Flash (Qwen Team, 2024; Grattafiori et al., 2024; Jiang et al., 2023; Kim et al., 2024; Gemma Team, 2025; Alexandru et al., 2025; DeepSeek-AI, 2026). Pairwise datasets use categorical direct-preference judge outputs; SummEval uses discrete scalar rubric bins. Arena100K is a filtered English non-tie LMArena-100K subset rather than an Arena leaderboard reproduction. All results use 30 grouped splits by source identifier. Each split contains a path-selection block, a calibration block of size  $n_M$ , a validation block, and a held-out test block; candidate paths are built on selection data, aggregators are fit on calibration data,  $(K, \mathcal{A})$  is selected on validation data, and test labels are used only for final evaluation and diagnostics.

The joint-table calibrator maps each observed judge-output pattern to a smoothed cell mean,  $(N_z \bar{Y}_z + \alpha \bar{y}_{\text{cal}})/(N_z + \alpha)$ , and backs off to the calibration marginal on unseen patterns. Scalar comparators include mean/vote aggregation with isotonic calibration, one-coin reliability aggregation, ridge stacking with isotonic calibration, logistic stacking for pairwise targets, and pairwise-feature variants (Platt, 1999; Guo et al., 2017; Wolpert, 1992). For scalar aggregators on pairwise tasks, verdicts are encoded as  $A/a = 1$ ,  $B/b = 0$ , and tie or parse-error outcomes as  $1/2$ ; the joint table keeps the categorical outputs as pattern values. This encoding makes simple mean/vote aggregation well behaved on RewardBench and Arena100K, while LLMBar still requires learned reliability or stacking weights. Appendix C adds a representative unsupervised heterogeneous-jury baseline, an NLL-selection ablation, split-proportion checks, and a hierarchical-backoff table. Each reported deployable comparison is an FCPS restriction to a candidate menu: joint-table only, scalar-family only, or the union of path and aggregator choices. MSE is the validation objective tied to the theory; NLL, accuracy, Pearson, and Spearman are robustness checks reported in the appendix.

## 5 Results

The empirical results make the finite-calibration map concrete. First, within the joint-table restriction of FCPS, risk over  $K$  often flattens or turns upward, and selected prefixes are usually smaller than the full seven-judge pool (Appendix Figures 1–3). Table 2 tracks cell pressure: it falls with more labels, while the

Dataset	$n_M$	$\hat{K}$	$\sum \hat{p}_z/N_z$	$\hat{u}$	$\hat{V}^{cell}$	proxy $\tilde{V}$	table	scalar
RewardBench	50	2.57	0.07510	0.0334	0.10855	0.0885	0.0259	0.0238
RewardBench	800	3.63	0.02282	0.0077	0.03049	0.0127	0.0251	0.0225
LLMBar	20	2.37	0.21937	0.1020	0.32137	0.3266	0.2257	0.2285
LLMBar	300	4.13	0.09100	0.0292	0.12017	0.0749	0.2031	0.1857
SummEval	32	1.47	0.24489	0.0746	0.31946	0.2565	0.0559	0.0511
SummEval	800	2.47	0.06106	0.0169	0.07799	0.0474	0.0454	0.0435
Arena100K	50	2.43	0.10241	0.0405	0.14291	0.1129	0.2395	0.2383
Arena100K	400	2.73	0.03033	0.0067	0.03700	0.0195	0.2331	0.2324

Table 2: Post-selection held-out audit of cell pressure for the validation-selected joint-table candidate. The column  $\hat{V}^{cell} = \sum_{z:N_z>0} \hat{p}_{test}(z)/N_z + \hat{u}$  directly instantiates the two terms in Eq. (7) using calibration cell counts and held-out test pattern frequencies. It is diagnostic only and is not used to select the deployed family. The proxy  $\tilde{V} = H_{\hat{K}}/n_M + \hat{u}$  is shown for comparison, followed by the validation-selected joint-table and scalar-family test risks.

Method	RewardBench	LLMBar	SummEval	Arena100K
Best single judge (val.)	0.032 $\pm$ 0.001	0.219 $\pm$ 0.004	0.045 $\pm$ 0.001	0.234 $\pm$ 0.002
All seven judges	0.028 $\pm$ 0.001	0.211 $\pm$ 0.002	0.059 $\pm$ 0.001	0.245 $\pm$ 0.002
Information-first + val. $K$	0.024 $\pm$ 0.001	0.204 $\pm$ 0.002	0.044 $\pm$ 0.001	0.231 $\pm$ 0.002
Complexity-penalized + val. $K$	0.025 $\pm$ 0.001	0.204 $\pm$ 0.002	0.046 $\pm$ 0.001	0.232 $\pm$ 0.002
Random path + val. $K$	0.027 $\pm$ 0.001	0.207 $\pm$ 0.003	0.048 $\pm$ 0.001	0.240 $\pm$ 0.002
Path-family envelope	0.025 $\pm$ 0.001	0.203 $\pm$ 0.002	0.045 $\pm$ 0.001	0.233 $\pm$ 0.002
Test oracle envelope	0.022 $\pm$ 0.001	0.194 $\pm$ 0.002	0.043 $\pm$ 0.001	0.227 $\pm$ 0.002

Table 3: Baseline and envelope test risk at each dataset’s largest available calibration budget. Values are mean  $\pm$  standard error over splits. The path-family envelope selects the path rule and prefix size by validation risk within each split and fixed budget; the test oracle envelope is a non-deployable diagnostic upper bound. No calibration budget is selected using test risk.

entropy proxy can understate literal small-cell pressure.

Second, current real benchmarks often look additive or redundant enough for low-dimensional calibration to be the better finite-label investment: scalar aggregation wins 16 of 20 dataset–budget comparisons against joint-table prefix calibration, with paired 95% intervals excluding zero in 11 cells (Appendix Table 11). Tables pay estimation cost when judge outputs lack enough interaction gain. Appendix Table 10 shows that family choice is the larger real-data effect, while prefix selection mainly protects joint tables from all-seven support pressure.

Third, controlled and semi-real interaction stress tests show the opposite regime. In the six-way parity dataset, the selected table uses  $K = 6$ , unseen mass falls from 0.768 at  $n_M = 16$  to zero by  $n_M = 512$ , and test MSE drops from 0.224 to 0.061; the +0.053 entry in Table 22 is the scalar-minus-table gap at  $n_M = 1024$ . Appendix C also reports robustness checks and cold-start deployment, where guarded selection defaults to a task-type prior unless few-label validation supports adaptation.

## 6 Conclusion

Judge-panel design is a finite-calibration problem: a stronger judge or larger pool can improve information, but it also changes the calibration object estimated from human labels. The deployment question is whether the next judge exposes structure that the available labels can learn.

The regime map makes that question operational. On current real benchmarks, scalar and reliability

aggregators often capture most useful signal; in controlled and semi-real interaction regimes, joint tables become valuable once unseen mass and small-cell pressure fall. FCPS validates over a compact menu and audits whether the selected complexity is supported by finite labels. Panels should expand only when they buy estimable structure.

## References

- Firoj Alam, Gagan Bhatia, Sahinur Rahman Laskar, and Shammur Absar Chowdhury. Beyond LLM-as-a-judge: Deterministic metrics for multilingual generative text evaluation. arXiv:2604.05083, 2026.
- Andrei Alexandru, Antonia Calvi, Henry Broomfield, Jackson Golden, Kyle Dai, Mathias Leys, Maurice Burger, Max Bartolo, Roman Engeler, Sashank Pisupati, Toby Drane, and Young Sun Park. Atla Selene Mini: A general purpose evaluation model. arXiv:2501.17195, 2025.
- Peter L. Bartlett and Shahar Mendelson. Rademacher and Gaussian complexities: Risk bounds and structural results. *Journal of Machine Learning Research*, 3:463–482, 2002.
- Maxim Khomiakov and Jes Frellsen. Noise-response calibration: A causal intervention protocol for LLM-judges. arXiv:2603.17172, 2026.
- Sher Badshah, Ali Emami, and Hassan Sajjad. SCOPE: Selective conformal optimized pairwise LLM judging. arXiv:2602.13110, 2026.
- Wei-Lin Chiang, Lianmin Zheng, Ying Sheng, Anastasios N. Angelopoulos, Tianle Li, Dacheng Li, Hao Zhang, Banghua Zhu, Michael I. Jordan, Joseph E. Gonzalez, and Ion Stoica. Chatbot Arena: An open platform for evaluating LLMs by human preference. arXiv:2403.04132, 2024.
- A. Philip Dawid. The well-calibrated Bayesian. *Journal of the American Statistical Association*, 77(379):605–610, 1982.
- A. Philip Dawid and Allan M. Skene. Maximum likelihood estimation of observer error-rates using the EM algorithm. *Applied Statistics*, 28(1):20–28, 1979.
- Hamid Dadkhahi, Firas Trabelsi, Parker Riley, Juraj Juraska, and Mehdi Mirzazadeh. Distribution-calibrated inference time compute for thinking LLM-as-a-judge. arXiv:2512.03019, 2025.
- DeepSeek-AI. DeepSeek-V4: Towards highly efficient million-token context intelligence. Model card and technical report, 2026. <https://huggingface.co/deepseek-ai/DeepSeek-V4-Flash>.
- Alexander R. Fabbri, Wojciech Kryscinski, Bryan McCann, Caiming Xiong, Richard Socher, and Dragomir Radev. SummEval: Re-evaluating summarization evaluation. *Transactions of the Association for Computational Linguistics*, 9:391–409, 2021.
- Chen Feng, Minghe Shen, Ananth Balashankar, Carsten Gerner-Beuerle, and Miguel R. D. Rodrigues. Noisy but valid: Robust statistical evaluation of LLMs with imperfect judges. In *Proceedings of ICLR*, 2026.
- Gemma Team. Gemma 3 technical report. arXiv:2503.19786, 2025.
- Aaron Grattafiori et al. The Llama 3 herd of models. arXiv:2407.21783, 2024.
- Chuan Guo, Geoff Pleiss, Yu Sun, and Kilian Q. Weinberger. On calibration of modern neural networks. In *Proceedings of the 34th International Conference on Machine Learning*, 2017.

- László Györfi, Michael Kohler, Adam Krzyżak, and Harro Walk. *A Distribution-Free Theory of Nonparametric Regression*. Springer, 2002.
- Helia Hashemi, Jason Eisner, Corby Rosset, Benjamin Van Durme, and Chris Kedzie. LLM-Rubric: A multidimensional, calibrated approach to automated evaluation of natural language texts. In *Proceedings of ACL*, 2024.
- Wassily Hoeffding. Probability inequalities for sums of bounded random variables. *Journal of the American Statistical Association*, 58(301):13–30, 1963.
- Suryaansh Jain, Umair Z. Ahmed, Shubham Sahai, and Ben Leong. Beyond consensus: Mitigating the agreeableness bias in LLM judge evaluations. arXiv:2510.11822, 2025.
- Albert Q. Jiang, Alexandre Sablayrolles, Arthur Mensch, Chris Bamford, Devendra S. Chaplot, Diego de las Casas, Florian Bressand, Gianna Lengyel, Guillaume Lample, Lucile Saulnier, Léo Renard Lavaud, Marie-Anne Lachaux, Pierre Stock, Teven Le Scao, Thibaut Lavril, Thomas Wang, Timothée Lacroix, and William El Sayed. Mistral 7B. arXiv:2310.06825, 2023.
- Seungone Kim, Juyoung Suk, Shayne Longpre, Bill Yuchen Lin, Jamin Shin, Sean Welleck, Graham Neubig, Moontae Lee, Kyungjae Lee, and Minjoon Seo. Prometheus 2: An open source language model specialized in evaluating other language models. In *Proceedings of EMNLP*, 2024.
- Nathan Lambert, Valentina Pyatkin, Jacob Morrison, LJ Miranda, Bill Yuchen Lin, Khyathi Chandu, Nouha Dziri, Sachin Kumar, Tom Zick, Yejin Choi, Noah A. Smith, and Hannaneh Hajishirzi. RewardBench: Evaluating reward models for language modeling. arXiv:2403.13787, 2024.
- Eddie Landesberg and Manjari Narayan. Causal judge evaluation: Calibrated surrogate metrics for LLM systems. arXiv:2512.11150, 2025.
- Ryan Lail and Luke Markham. On cost-effective LLM-as-a-judge improvement techniques. arXiv:2604.13717, 2026.
- Yanran Li. Calibrate, don’t curate: Label-efficient estimation from noisy LLM judges. arXiv:2605.09702, 2026.
- Yang Liu, Dan Iter, Yichong Xu, Shuohang Wang, Ruochen Xu, and Chenguang Zhu. G-Eval: NLG evaluation using GPT-4 with better human alignment. In *Proceedings of EMNLP*, 2023.
- John C. Platt. Probabilistic outputs for support vector machines and comparisons to regularized likelihood methods. In *Advances in Large Margin Classifiers*, 1999.
- Qwen Team. Qwen2.5 technical report. arXiv:2412.15115, 2024.
- Mengjie Qian, Guangzhi Sun, Mark J. F. Gales, and Kate M. Knill. Who can we trust? LLM-as-a-jury for comparative assessment. arXiv:2602.16610, 2026.
- Bhaktipriya Radharapu, Eshika Saxena, Kenneth Li, Chenxi Whitehouse, Adina Williams, and Nicola Cancedda. Calibrating LLM judges: Linear probes for fast and reliable uncertainty estimation. arXiv:2512.22245, 2025.
- Huanxin Sheng, Xinyi Liu, Hangfeng He, Jieyu Zhao, and Jian Kang. Analyzing uncertainty of LLM-as-a-judge: Interval evaluations with conformal prediction. In *Proceedings of EMNLP*, 2025.

- Mervyn Stone. Cross-validators choice and assessment of statistical predictions. *Journal of the Royal Statistical Society: Series B*, 36(2):111–133, 1974.
- Kelly Tang, Wei-Lin Chiang, and Anastasios N. Angelopoulos. Arena Explorer: A topic modeling pipeline for LLM evals and analytics. Dataset citation for `lmarena-ai/arena-human-preference-100k`, 2025.
- David H. Wolpert. Stacked generalization. *Neural Networks*, 5(2):241–259, 1992.
- Shibo Yu, Yingzhou Wang, Yan Chen, Guodong Li, and Jin-Hong Du. Heterogeneous judge-aware ranking with sensitivity, disagreement, and confidence. `arXiv:2605.05073`, 2026.
- Zhiyuan Zeng, Jiatong Yu, Tianyu Gao, Yu Meng, Tanya Goyal, and Danqi Chen. Evaluating large language models at evaluating instruction following. In *Proceedings of ICLR*, 2024.
- Pat Verga, Sebastian Hofstätter, Sophia Althammer, Yixuan Su, Aleksandra Piktus, Arkady Arkhangorodsky, Minjie Xu, Naomi White, and Patrick Lewis. Replacing judges with juries: Evaluating LLM generations with a panel of diverse models. `arXiv:2404.18796`, 2024.
- Lianghui Zhu, Xinggang Wang, and Xinlong Wang. JudgeLM: Fine-tuned large language models are scalable judges. `arXiv:2310.17631`, 2023.
- Lianmin Zheng, Wei-Lin Chiang, Ying Sheng, Siyuan Zhuang, Zhanghao Wu, Yonghao Zhuang, Zi Lin, Zhuohan Li, Dacheng Li, Eric P. Xing, Hao Zhang, Joseph E. Gonzalez, and Ion Stoica. Judging LLM-as-a-judge with MT-Bench and Chatbot Arena. In *Advances in Neural Information Processing Systems*, 2023.

## A Limitations

The current evidence maps a fixed deployment regime. The real study uses a seven-judge pool and deterministic judge outputs; broader tests should swap judges, increase pool diversity, and use multiple stochastic samples per judge. Many benchmarks appear additive or redundant, and some gains are small. The theory-proxy diagnostic matches 16 of 20 dataset–budget cells, while split-level discrimination remains modest. The appendix includes a representative Dawid–Skene/BT-style jury baseline, hierarchical backoff, and residual-shrinkage diagnostics, and leaves full BT variants, conformal abstention, dynamic jury selection, and more expressive higher-order stackers for future comparison. Many heterogeneous-jury methods infer latent item quality or unsupervised judge reliability from comparison graphs rather than calibrating fixed judge-output patterns to human labels. Larger, more heterogeneous judge pools are needed to test how the regime tradeoff scales.

## B Proofs

**Proof of Theorem 1.** Hoeffding’s inequality and a union bound give  $\sup_{c \in \mathcal{C}} |\widehat{\mathcal{R}}_{\text{val}}(\widehat{f}_c) - \mathcal{R}(\widehat{f}_c)| \leq \epsilon$  with  $\epsilon = \sqrt{\log(2|\mathcal{C}|/\delta)/(2n_V)}$ . The validation argmin then satisfies  $\mathcal{R}(\widehat{f}_{\widehat{c}}) \leq \widehat{\mathcal{R}}_{\text{val}}(\widehat{f}_{\widehat{c}}) + \epsilon \leq \widehat{\mathcal{R}}_{\text{val}}(\widehat{f}_c) + \epsilon \leq \mathcal{R}(\widehat{f}_c) + 2\epsilon$  for every  $c \in \mathcal{C}$ .

**Proof of Proposition 1.** The first display follows from Hoeffding’s inequality and a union bound over occupied cells. For squared loss,  $\mathcal{R}(\tilde{g}) - \mathcal{R}(g^*) = \mathbb{E}[(\tilde{g}(Z_K) - g^*(Z_K))^2]$  on any fixed deployed predictor. On occupied cells,  $|\tilde{g}(z) - g^*(z)| \leq |\bar{Y}_z - g^*(z)| + \alpha/(N_z + \alpha)$ , and  $(a + b)^2 \leq 2a^2 + 2b^2$ . On unseen cells, both predictions lie in  $[0, 1]$ , so the squared contribution is at most the unseen probability  $u_K$ . Integrating these cellwise bounds with respect to the test-time probabilities  $p_z$  gives the weighted terms in Eq. (6).

**Proof sketch of Proposition 2.** The lower balance condition and a Chernoff bound imply  $N_z \geq n_M/(2cM_K)$  for all cells with probability at least  $1 - \delta$  once  $n_M$  is a sufficiently large multiple of  $cM_K \log(M_K/\delta)$ . Substituting this count lower bound and  $p_z \leq c/M_K$  into Eq. (6) gives Eq. (8); the same event sets the unseen-mass term to zero. The lower bound is the standard finite-dimensional mean-estimation lower bound: under balanced sampling, estimating  $M_K$  unrelated conditional means from  $n_M$  labels incurs total weighted variance of order  $M_K/n_M$ .

**Proof sketch of Proposition 3.** The empirical Rademacher complexity of bounded linear functions on  $[0, 1]^K$  with  $\|w\|_2 \leq B$  is  $O(B\sqrt{K/n_M})$ . The contraction inequality transfers this rate through the Lipschitz link and an  $L$ -Lipschitz loss, and the standard uniform convergence bound gives Eq. (10). Ridge and logistic stacking are regularized implementations of this low-dimensional family.

## C Extended Empirical Results

**Dataset construction.** RewardBench uses the first 1000 source preference rows from `allenai/reward-bench`; each chosen–rejected pair is expanded into original and swapped orders, giving 2000 position-balanced pairwise rows. LLMBench uses all five official subsets (Natural, Neighbor, GPTInst, GPTOut, and Manual), likewise expanded to original and swapped orders, giving 838 rows. SummEval uses the test split of `mteb/summeval`; each machine summary is labeled by the human coherence score normalized from the original 1–5 rubric to  $[0, 1]$ , giving 1600 scalar rows. Arena100K uses `lmarena-ai/arena-human-preference-100k`: we keep English non-tie rows, skip examples whose user plus two assistant conversations exceed an estimated 5000 tokens, retain 800 source conversations, and create original and swapped pairwise rows for 1600 total rows. For all position-balanced pairwise datasets, grouped splits use the original source id (`id`, `question_id`, or constructed LLMBench id) so swapped copies of the same comparison cannot cross selection, calibration, validation, and test blocks.

**SummEval discretization.** SummEval labels are the human coherence scores normalized from the original 1–5 rubric to  $[0, 1]$ . Judge outputs for SummEval use the direct scalar schema: each judge is prompted for a score in  $\{1, 2, 3, 4, 5\}$ , and any parsed numeric response is rounded and clipped to that range before entering the joint pattern table. Thus table sparsity on SummEval is driven by products of five-level judge bins rather than pairwise verdict alphabets. Table 18 checks that the largest-budget joint-table conclusion is stable across smoothing and fallback choices; sensitivity to alternative rubric binnings remains a natural extension.

**Judge configuration and deterministic outputs.** The fixed judge pool uses Qwen2.5-7B-Instruct (Qwen Team, 2024), Llama-3.1-8B-Instruct (Grattafiori et al., 2024), Mistral-7B-Instruct-v0.3 (Jiang et al., 2023), Prometheus-7B-v2.0 (Kim et al., 2024), Gemma-3-12B-IT (Gemma Team, 2025), Selene-1-Mini-Llama-3.1-8B (Alexandru et al., 2025), and DeepSeek V4 Flash (DeepSeek-AI, 2026). All seven judge outputs use a direct schema: pairwise tasks request a JSON verdict in  $\{A, B, \text{tie}\}$ , and SummEval requests a JSON score in  $\{1, \dots, 5\}$ . Local vLLM and transformers runs use deterministic decoding with temperature 0 or

Block	Used for	Not used for
Selection block	Construct judge paths and path-specific oracle diagnostics	Fitting calibration maps or reporting final risk
Calibration block	Fit table, stacking, one-coin, and calibration maps	Choosing the final candidate by test performance
Validation block	Select $K$ , path, and/or aggregator family within a split	Estimating final held-out performance
Test block	Report final risk and diagnostics after selection is fixed	Choosing budget, $K$ , path, aggregator, smoothing, or fallback

Table 4: Protocol guardrails. All deployed choices are made before the test block is evaluated. Tables that compare budgets or families report either fixed largest-budget results or validation-selected choices, avoiding test-informed model selection.

`do_sample=False`; the DeepSeek API anchor uses temperature 0, JSON response formatting, and non-thinking mode. We treat each judge as a deterministic annotator for this paper. Repeated stochastic samples per judge would create a different candidate family and are left to jury/repeated-sample methods.

**Prompt and parsing details.** For generic pairwise judges, the system message is “You are a strict preference judge. Return only valid JSON,” and the user prompt asks which response is better for the original user prompt, preferring helpful, correct, harmless, and instruction-following answers, then requires exactly `{'verdict': 'A' | 'B' | 'tie'}`. For SummEval-style scalar judges, the system message is “You are a strict summary-evaluation judge. Return only valid JSON,” and the user prompt asks for an integer 1–5 score on the requested dimension, with 1 meaning very poor and 5 excellent. Prometheus uses its recommended feedback-style prompt with a final `[RESULT]` marker, but the parsed output is collapsed to the same verdict or score alphabet. Local runs use `max_tokens = 80` for generic prompts and 128–512 for Prometheus-style feedback prompts; DeepSeek uses `max_tokens = 80`, JSON response formatting, up to three retries, and no prompt paraphrase or decoding-seed sweep. Parsed scalar scores are rounded and clipped to  $\{1, \dots, 5\}$ ; invalid categorical verdicts fall back to tie, while unparseable outputs are recorded as `parse_error`. When these categorical pairwise outputs are used by scalar aggregators,  $A/a$  is mapped to 1,  $B/b$  to 0, and both tie and `parse_error` to  $1/2$ ; the joint-table family instead treats each recorded output category as a distinct cell value.

## C.1 Calibration-Frontier Path Diagnostic

We evaluated a calibration-frontier path generator that ranks judge subsets by selection-block oracle gain and exact binomial estimates of the cell-pressure term in Eq. (7), keeps a capped Pareto frontier (`cfps_max_paths = 32`), and then applies the same validation selector. Table 20 compares this generator against the original split-wise validation envelope over accuracy, gain-complexity, and random paths. The result is a calibration-frontier diagnostic: CFPS wins some low-budget cells, while the information-first path remains competitive across datasets. The essential decision is validation over prefix size and aggregation family under finite calibration labels.

## C.2 Cold-Start Few-Label Diagnostic

We also simulate a deployment setting in which the dataset itself is a new target task and the only prior information is task type. For each real benchmark we expose only  $n_h \in \{8, 16, 32, 64\}$  grouped target labels for selection and calibration, then evaluate on a held-out grouped test block. The task-type prior uses

Theory component	Empirical evidence	Interpretation
Validation selector over $(K, \mathcal{A})$	Tables 3–11	Selection is evaluated without test-informed budget or model-family choice.
Joint-table support term $H_K/n_M$ and unseen mass	Figures 1, 4, 5; Table 26	Old prefix figures are diagnostics for the joint-table family, not claims about all aggregators.
Operational table-pressure instantiation	Table 2	Calibration cell counts and held-out pattern frequencies instantiate the plug-in cell-pressure term $\sum_z \hat{p}_z/N_z + \hat{u}$ , with $H_K/n_M + \hat{u}$ shown only as a proxy.
Low-dimensional/reliability aggregators plus approximation bias	Tables 8–12; Table 11	Scalar aggregation and one-coin reliability models often win on real benchmarks because they avoid the joint pattern table, and this is checked across MSE, NLL, accuracy, and correlation metrics.
Theory proxies for family choice	Table 17	$H_K/n_M$ , unseen rate, and pairwise gain provide an exploratory, modestly discriminative check rather than confirmatory winner prediction.
Smoothing and fallback terms in the table bound	Table 18	Joint-table conclusions are checked against alternative smoothing constants and lower-prefix fallback.
Approximation–estimation regime distinction	Table 24	Additive regimes favor stacking; interaction regimes can favor the joint table when labels are sufficient.

Table 5: How the revised  $(K, \mathcal{A})$  theory is supported empirically. The previous figures remain useful, but they should be read as joint-table diagnostics; aggregator-level evidence comes from scalar baselines, regime comparisons, and controlled additive/interaction experiments.

one-coin reliability for pairwise tasks and ridge calibration for scalar tasks. Naive FCPS always deploys the cross-validated selector over path, prefix size, and aggregator; guarded FCPS deviates from the prior only when the selected candidate’s cross-validated upper one-SE risk is below the prior’s lower one-SE risk. Table 21 shows that this extreme low-label setting is mostly a prior-dominated regime: the guard avoids most of the damage from naive selection, but rarely improves on the task-type prior. We therefore treat cold-start selection as a separate deployment problem rather than evidence that the full FCPS menu should be used with only a handful of target labels.

### C.3 New Calibration-Growth Dataset

To isolate the effect of increasing calibration labels, we generated a fresh JSONL panel dataset with seven binary judges and three regimes: additive, mixed, and six-way parity. We then increased the calibration budget from 16 to 2048 labels and compared validation-selected prefix sizes within a joint-table family, an additive ridge family, and a pairwise-ridge family. Table 22 reports the best scalar risk minus the joint-table

Interpretation question	Evidence check	Takeaway
What does validation select?	Theorem 1; Tables 5 and 10	Validation is the selection primitive; the contribution is the finite-calibration candidate space, diagnostics, and regime evidence.
Does $K$ -selection matter beyond family choice?	Table 10; Figure 8	Family choice is the larger real-data effect; prefix selection mainly protects joint tables from all-seven support pressure.
Are conclusions MSE-specific?	Tables 12 and 14	The scalar/reliability pattern also appears under non-MSE metrics, with MSE as the theory-aligned objective.
Are there middle families between scalars and full tables?	Tables 15 and 19	Backoff and residual-shrinkage variants are diagnostic middle points with limited gains over the strongest scalar selector.
Is the path heuristic essential?	Table 20; Figure 7	Path choice affects some cells, while the prefix/family decision remains the main finite-calibration object.
How should table diagnostics be read?	Table 2; Table 17; Figures 4–5	$H_K/n_M$ is an exploratory pressure proxy; exact cell pressure and unseen mass provide the closer audit quantities.
Does SummEval binning drive the result?	Appendix “SummEval discretization”; Table 18	The fixed five-bin schema is documented, smoothing/fallback sensitivity is checked, and alternative binnings remain future work.
How far does the fixed judge pool generalize?	Appendix “Judge configuration and deterministic outputs”; Limitations	The study covers a fixed deployed pool; larger heterogeneous and stochastic pools are future work.

Table 6: Navigation map from interpretation questions to the corresponding evidence checks in the draft. Several checks are diagnostics that clarify the operating regime rather than separate algorithmic components.

Dataset	reporting budget $n_M$	envelope risk	envelope mean $K$
RewardBench	800	$0.025 \pm 0.001$	3.63
LLMBar	300	$0.203 \pm 0.002$	4.13
SummEval	800	$0.045 \pm 0.001$	2.47
Arena100K	400	$0.233 \pm 0.002$	2.73

Table 7: Fixed reporting budget and selected complexity for the validation-selected path-family envelope used in Table 3. The reporting budget is the largest available calibration budget for each dataset.

risk. The additive regime remains scalar-favored at moderate and large budgets. In contrast, the mixed and parity regimes favor the table: for the parity regime, the selected table uses  $K = 6$ , its held-out unseen-pattern rate falls from 0.768 at  $n_M = 16$  to 0 by  $n_M = 512$ , and its test MSE falls from 0.224 to 0.061 at that budget. The  $+0.053$  table entry at  $n_M = 1024$  is the scalar-minus-table gap, not the table risk. This is the clean positive counterpart to the real-benchmark results: once the target truly contains a high-order interaction, additional calibration labels can make the nonparametric aggregator worthwhile.

#### C.4 Semi-Real Pattern Calibration-Growth Dataset

To make the interaction stress test less stylized, we also construct a semi-real dataset by resampling seven-judge output patterns from the real RewardBench, LLMBar, and Arena100K panels, then assigning controlled additive, mixed, and parity targets to those real patterns. This preserves the empirical judge correlations and pattern sparsity while letting us know whether the target contains an interaction. Table 23 shows the expected boundary: additive targets become scalar-favored after the smallest budgets, while mixed and parity targets favor the joint table. In the parity regime, the selected table keeps  $K \approx 6$ , unseen rate falls

Method	RewardBench	LLMBar	SummEval	Arena100K
All-judge mean + isotonic	$0.022 \pm 0.001$	$0.245 \pm 0.002$	$0.047 \pm 0.001$	$0.231 \pm 0.001$
One-coin reliability + isotonic	$0.021 \pm 0.001$	$0.195 \pm 0.003$	$0.050 \pm 0.001$	$0.229 \pm 0.002$
Ridge stacking + isotonic	$0.023 \pm 0.001$	$0.184 \pm 0.002$	$0.043 \pm 0.001$	$0.231 \pm 0.002$
Logistic stacking	$0.021 \pm 0.001$	$0.181 \pm 0.002$	$0.059 \pm 0.001$	$0.228 \pm 0.002$
Ridge pairwise stacking + isotonic	$0.025 \pm 0.001$	$0.192 \pm 0.002$	$0.044 \pm 0.001$	$0.237 \pm 0.002$
Logistic pairwise stacking	$0.021 \pm 0.001$	$0.183 \pm 0.002$	$0.060 \pm 0.001$	$0.229 \pm 0.002$

Table 8: Scalar aggregation baselines at each dataset’s largest calibration budget. All methods use all seven judge outputs and avoid the full joint pattern table. Pairwise verdicts are encoded as  $A/a = 1$ ,  $B/b = 0$ , and tie or parse-error outcomes as  $1/2$  before fitting scalar models. The reported metric is mean squared calibration error, matching Table 3.

Dataset	$n_M$	selected aggregation family	selected $K$	test MSE
RewardBench	800	Logistic pairwise (0.23)	6.17	$0.023 \pm 0.001$
LLMBar	300	Logistic (0.43)	7.00	$0.183 \pm 0.002$
SummEval	800	Ridge + isotonic (0.63)	6.70	$0.044 \pm 0.001$
Arena100K	400	One-coin reliability + isotonic (0.43)	6.53	$0.232 \pm 0.002$

Table 9: Validation-selected scalar aggregation at each dataset’s largest calibration budget. The selector chooses both aggregation family and prefix size using validation risk within each split; the parenthesized value is the split share of the most frequently selected family.

from 0.273 at  $n_M = 16$  to 0.007 at  $n_M = 2048$ , and the table advantage remains positive.

## D Additional Diagnostics

### D.1 Path-Separated Complexity Diagnostic

Figure 7 repeats the complexity-pressure diagnostic separately for each path rule. The pooled trend in Figure 4 is not driven by a single path alone: most cells show that higher effective support per calibration label corresponds to higher median risk or wider risk tails. Path-specific risk-complexity behavior differs by dataset, and the information-first path remains a strong practical baseline.

### D.2 Marginal Stopping Diagnostic

Equation (1) suggests a marginal stopping principle. A new judge should be added only when its marginal oracle-information gain exceeds its calibration-complexity cost. Figure 8 visualizes this principle by plotting the change in test risk from  $K$  to  $K + 1$  against the corresponding increase in complexity pressure. Points below zero are beneficial additions. The median trend is close to zero and the tails widen as marginal complexity increases, indicating that extra judges do not reliably improve finite risk.

### D.3 Uncertainty Diagnostics

Dataset	$n_M$	table $K=7$	table sel. $K$	scalar $K=7$	scalar sel. $K$	full $K=7$	full sel. $K$
RewardBench	800	0.0277	0.0251	0.0218	0.0225	0.0218	0.0234
LLMBar	300	0.2110	0.2031	0.1857	0.1857	0.1863	0.1886
SummEval	800	0.0588	0.0454	0.0433	0.0435	0.0433	0.0436
Arena100K	400	0.2448	0.2331	0.2316	0.2324	0.2318	0.2318

Table 10:  $K$ -versus-family ablation at each dataset’s largest calibration budget. All entries are split-wise validation selectors over existing candidates, reported as mean test MSE. “table  $K=7$ ” fixes the all-seven joint table; “table sel.  $K$ ” selects the table prefix by validation risk; “scalar  $K=7$ ” selects the scalar family at the all-seven prefix; “scalar sel.  $K$ ” selects both scalar family and prefix; “full” pools joint-table and scalar candidates. The main real-data gain comes from choosing an estimable aggregation family rather than from scalar-family prefix selection alone, while prefix selection protects the joint table from all-seven support pressure.

Dataset	$n_M$	table	scalar	$\Delta$	paired 95% CI
RewardBench	50	0.0252	0.0219	0.0033	[0.0013,0.0053]
RewardBench	100	0.0249	0.0225	0.0025	[0.0012,0.0038]
RewardBench	200	0.0251	0.0220	0.0032	[0.0017,0.0046]
RewardBench	400	0.0243	0.0217	0.0026	[0.0015,0.0037]
RewardBench	800	0.0240	0.0227	0.0014	[-0.0001,0.0028]
LLMBar	20	0.2254	0.2212	0.0042	[-0.0036,0.0120]
LLMBar	50	0.2213	0.2111	0.0102	[0.0033,0.0171]
LLMBar	100	0.2147	0.1972	0.0176	[0.0126,0.0226]
LLMBar	200	0.2104	0.1914	0.0189	[0.0123,0.0256]
LLMBar	300	0.2039	0.1826	0.0214	[0.0186,0.0241]
SummEval	32	0.0569	0.0511	0.0058	[0.0032,0.0084]
SummEval	64	0.0528	0.0501	0.0026	[0.0004,0.0048]
SummEval	128	0.0485	0.0474	0.0011	[-0.0006,0.0028]
SummEval	256	0.0451	0.0460	-0.0009	[-0.0022,0.0005]
SummEval	512	0.0448	0.0436	0.0011	[0.0002,0.0021]
SummEval	800	0.0444	0.0435	0.0009	[-0.0001,0.0019]
Arena100K	50	0.2383	0.2372	0.0011	[-0.0033,0.0056]
Arena100K	100	0.2326	0.2349	-0.0023	[-0.0056,0.0010]
Arena100K	200	0.2328	0.2331	-0.0003	[-0.0035,0.0029]
Arena100K	400	0.2311	0.2321	-0.0010	[-0.0045,0.0026]

Table 11: Cross-budget regime comparison. The table column uses the lowest-risk validation-selected path rule within the joint-table family; the scalar column uses validation to select scalar aggregation family and prefix size at the same budget. Here  $\Delta$  is table risk minus scalar risk, so positive values favor scalar aggregation. Paired intervals are normal 95% intervals over the 30 split-wise differences for the same fixed table rule and scalar selector.

Dataset	MSE	NLL	Accuracy	Pearson	Spearman
RewardBench	0.023 $\pm$ 0.001	0.101 $\pm$ 0.005	0.971 $\pm$ 0.001	0.954 $\pm$ 0.002	0.914 $\pm$ 0.003
LLMBar	0.183 $\pm$ 0.002	0.557 $\pm$ 0.010	0.719 $\pm$ 0.006	0.522 $\pm$ 0.008	0.522 $\pm$ 0.008
SummEval	0.044 $\pm$ 0.001	0.621 $\pm$ 0.002	0.763 $\pm$ 0.004	0.601 $\pm$ 0.007	0.592 $\pm$ 0.007
Arena100K	0.232 $\pm$ 0.002	0.665 $\pm$ 0.006	0.626 $\pm$ 0.006	0.273 $\pm$ 0.012	0.273 $\pm$ 0.013

Table 12: Metric robustness for validation-selected scalar aggregation at the largest calibration budget. MSE is the main paper metric; NLL, accuracy, Pearson correlation, and Spearman correlation check that the scalar-aggregation finding is not only an MSE artifact.

Dataset	joint table	scalar selector	DS/BT-style jury	selected $K$
Arena100K	0.233	0.232	$0.235 \pm 0.002$	6.07
LLMBar	0.203	0.183	$0.238 \pm 0.002$	2.33
RewardBench	0.025	0.023	$0.024 \pm 0.001$	6.10

Table 13: Representative heterogeneous unsupervised-jury baseline on pairwise tasks at the largest calibration budget. The DS/BT-style jury fits a Dawid–Skene one-coin model Dawid and Skene (1979) with judge-specific sensitivities and specificities from judge agreement, then orients and isotonic-calibrates the resulting score on the calibration labels; prefix size is selected by validation MSE. This is a representative reliability/jury baseline, not a full comparison to every BTJ or heterogeneous ranking model.

Dataset	$n_M$	MSE sel. MSE	NLL sel. MSE	MSE sel. NLL	NLL sel. NLL
Arena100K	50	0.237	0.237	0.697	0.676
Arena100K	100	0.235	0.235	0.697	0.670
Arena100K	200	0.233	0.232	0.702	0.670
Arena100K	400	0.232	0.232	0.665	0.664
LLMBar	20	0.221	0.221	0.704	0.632
LLMBar	50	0.211	0.210	0.647	0.621
LLMBar	100	0.197	0.198	0.635	0.647
LLMBar	200	0.191	0.191	0.607	0.578
LLMBar	300	0.183	0.184	0.557	0.559
RewardBench	50	0.022	0.020	0.123	0.094
RewardBench	100	0.022	0.022	0.139	0.109
RewardBench	200	0.022	0.022	0.115	0.108
RewardBench	400	0.022	0.021	0.106	0.095
RewardBench	800	0.023	0.022	0.101	0.096

Table 14: Pairwise scalar-selector sensitivity to the validation objective across calibration budgets. The candidate menu is unchanged; only the validation criterion changes from MSE to Bernoulli NLL.

Dataset	scalar	hier. backoff	sel.-heavy	default	val.-heavy
RewardBench	0.023	0.024	0.023	0.023	0.022
LLMBar	0.183	0.202	0.196	0.187	0.184
SummEval	0.044	0.043	0.045	0.044	0.044
Arena100K	0.232	0.230	0.233	0.233	0.231

Table 15: Two additional robustness checks at the largest calibration budget. The hierarchical-backoff column validates a prefix-smoothed table on the information-first path, selecting  $K$  and shrinkage by validation MSE. The last three columns rerun the scalar-family selector while shifting labels between the selection and validation blocks and keeping the calibration and test sizes fixed.

Dataset	additive risk	pairwise risk	pairwise-additive	pairwise selected
Arena100K	0.2316	0.2318	0.0002	0.10
LLMBar	0.1851	0.1846	-0.0005	0.57
RewardBench	0.0232	0.0232	-0.0000	0.17
SummEval	0.0431	0.0435	0.0004	0.33

Table 16: Real-data interaction diagnostic for scalar aggregation at the largest calibration budget. The additive column is the best all-seven ridge/logistic stacker; the pairwise column is the best all-seven stacker with second-order products. The last column reports the share of validation-selected scalar aggregators that use pairwise interaction features.

Diagnostic	Estimate	Uncertainty / test
Hard rule agreement over dataset-budget cells	16/20	one-sided binomial $p = 0.006$
Split-level proxy AUC for scalar winner	0.573	cluster bootstrap 95% CI [0.522, 0.624]
Within-cluster permutation test for AUC	–	$p = 0.002$
Scalar-minus-table proxy-score gap	0.476	cluster bootstrap 95% CI [0.221, 0.754]

Table 17: Statistical check for the theory-proxy winner diagnostic. The hard rule is evaluated only as a coarse aggregate sanity check. The split-level tests use the continuous proxy score  $z(H_K/n_M) + z(\text{unseen}) + z(\text{pairwise gain})$  to predict whether validation-selected scalar aggregation beats validation-selected table calibration on held-out test risk. Bootstrap resamples dataset-budget clusters; the permutation test shuffles winners within each dataset-budget cluster. These diagnostics are not used as a standalone selector.

Dataset	global fallback	lower-prefix fallback	best $\alpha$ /fallback
RewardBench	$0.024 \pm 0.001$	$0.024 \pm 0.001$	$\alpha = 2.0$ , lower-prefix: 0.023
LLMBar	$0.204 \pm 0.002$	$0.205 \pm 0.002$	$\alpha = 2.0$ , lower-prefix: 0.203
SummEval	$0.044 \pm 0.001$	$0.044 \pm 0.001$	$\alpha = 2.0$ , global: 0.044
Arena100K	$0.231 \pm 0.002$	$0.231 \pm 0.002$	$\alpha = 2.0$ , lower-prefix: 0.230

Table 18: Joint-table sensitivity at the largest calibration budget, using an information-first path and validation-selected prefix size. The table compares the default global-mean fallback against a lower-prefix fallback and reports the best alpha/fallback setting from the sweep. For SummEval, this sensitivity is after the fixed five-bin scalar judge discretization described in the appendix.

Dataset	table	scalar	residual-shrinkage	selected base
RewardBench	0.0251	0.0227	0.0223	one_coin_iso
LLMBar	0.2031	0.1826	0.1833	logistic
SummEval	0.0454	0.0435	0.0437	ridge_iso
Arena100K	0.2331	0.2321	0.2324	one_coin_iso

Table 19: Prototype residual-shrinkage hybrid at each dataset’s largest calibration budget. The method first fits a scalar baseline, then adds a count-shrunk residual table on joint output patterns and selects base family, prefix size, and shrinkage strength by validation risk. This diagnostic reports an intermediate family between scalar stackers and full joint tables.

Dataset	$n_M$	baseline	CFPS	+CFPS	$\Delta_+$	CFPS sel.
Arena100K	400	0.2331	0.2343	0.2341	+0.0010	0.77
LLMBar	300	0.2031	0.2043	0.2049	+0.0019	0.73
RewardBench	800	0.0251	0.0253	0.0260	+0.0009	0.67
SummEval	800	0.0454	0.0461	0.0461	+0.0007	0.73

Table 20: Calibration-frontier path search (CFPS) at each dataset’s largest calibration budget. The baseline is the split-wise validation envelope over accuracy, gain-complexity, and random paths; +CFPS adds the calibration-frontier candidates to the same validation envelope. Negative  $\Delta_+$  means the augmented menu has lower test risk.

Dataset	$n_h$	prior	naive FCPS	guarded FCPS	$\Delta_g$	guarded family
Arena100K	16	0.2670	0.2671	0.2686	+0.0016	One-coin reliability + isotonic (0.42)
Arena100K	64	0.2399	0.2467	0.2427	+0.0028	One-coin reliability + isotonic (0.25)
LLMBar	16	0.2600	0.2541	0.2560	-0.0040	One-coin reliability + isotonic (0.58)
LLMBar	64	0.2053	0.2135	0.2051	-0.0001	One-coin reliability + isotonic (0.08)
RewardBench	16	0.0340	0.0406	0.0340	+0.0000	One-coin reliability + isotonic (0.00)
RewardBench	64	0.0251	0.0323	0.0275	+0.0024	One-coin reliability + isotonic (0.17)
SummEval	16	0.0664	0.0781	0.0664	+0.0000	Ridge + isotonic (0.00)
SummEval	64	0.0513	0.0530	0.0518	+0.0005	Ridge + isotonic (0.17)

Table 21: Cold-start deployment with few human calibration labels over 12 random grouped splits. Each target dataset is treated as a new task; only  $n_h$  target labels are used for selection and calibration, then the selected predictor is refit on all  $n_h$  labels and evaluated on a held-out grouped test block. The prior baseline uses only task type: one-coin reliability for pairwise tasks and ridge calibration for scalar tasks. Naive FCPS always deploys the cross-validated selector. Guarded FCPS deviates from the task-type prior only when the selected candidate’s cross-validated upper one-SE risk is below the prior’s cross-validated lower one-SE risk. Negative  $\Delta_g$  favors guarded FCPS; the parenthetical entry is the adaptation rate.

Regime	16	64	256	1024	2048
Additive	-0.007	-0.003	-0.004	-0.002	-0.001
Mixed	<b>+0.014</b>	<b>+0.014</b>	<b>+0.043</b>	<b>+0.018</b>	<b>+0.010</b>
Parity	<b>+0.046</b>	<b>+0.101</b>	<b>+0.123</b>	<b>+0.053</b>	<b>+0.010</b>

Table 22: New calibration-growth dataset. Entries are mean test-MSE gaps after validation-selecting prefix size within each family: best scalar aggregator minus joint table. Positive values favor the joint table; bold marks gaps larger than 0.001. Thus the parity 0.053 entry at  $n_M = 1024$  is a gap, not the table risk. The additive regime remains scalar-favored, while the high-order parity regime tests when enough calibration labels are available for a nonparametric table to exploit interactions.

Regime	16	64	256	1024	2048
Additive	<b>+0.003</b>	+0.000	-0.001	-0.002	-0.001
Mixed	<b>+0.010</b>	<b>+0.005</b>	<b>+0.011</b>	<b>+0.006</b>	<b>+0.004</b>
Parity	<b>+0.065</b>	<b>+0.055</b>	<b>+0.030</b>	<b>+0.015</b>	<b>+0.009</b>

Table 23: Semi-real pattern calibration-growth dataset. Entries are mean test-MSE gaps after validation-selecting prefix size within each family: best scalar aggregator minus joint table. Positive values favor the joint table; bold marks gaps larger than 0.001. The judge-output patterns are resampled from real RewardBench, LLMBar, and Arena100K seven-judge outputs, while the target rule is controlled. Additive targets become scalar-favored after the smallest budgets; mixed and parity targets favor the joint table.

Regime	Budget	Joint table	Ridge + isotonic	Logistic
Additive	50	0.187	0.178	<b>0.171</b>
Additive	3000	0.159	0.158	<b>0.157</b>
XOR interaction	50	<b>0.140</b>	0.219	0.251
XOR interaction	3000	<b>0.117</b>	0.203	0.236
AND interaction	50	0.139	<b>0.137</b>	0.156
AND interaction	3000	<b>0.107</b>	0.115	0.129

Table 24: Controlled aggregator-regime experiment. Each entry is test MSE after selecting prefix size by validation within an aggregator family; bold marks the best family for that regime and budget. Additive signals favor low-dimensional stacking, while interaction signals favor the joint table once the calibration budget is large enough.

Interaction strength $\gamma$	$n_M = 50$	$n_M = 200$	$n_M = 1000$	$n_M = 3000$
0.0	-0.024	-0.013	-0.003	+0.000
0.3	-0.020	<b>+0.008</b>	<b>+0.014</b>	<b>+0.012</b>
0.5	<b>+0.046</b>	<b>+0.053</b>	<b>+0.056</b>	<b>+0.056</b>
0.7	<b>+0.110</b>	<b>+0.117</b>	<b>+0.117</b>	<b>+0.135</b>
1.0	<b>+0.171</b>	<b>+0.186</b>	<b>+0.182</b>	<b>+0.188</b>

Table 25: Interaction-strength sweep. Entries are mean test-MSE gaps after validation selection within each family: best scalar aggregator minus joint table. Positive values mean the joint table has lower risk; values above 0.001 are bolded. As interaction strength and calibration budget grow, the winner shifts from low-dimensional scalar aggregation toward the joint table.

Diagnostic	Estimate	SE	controlled units
$H_K/n_M \rightarrow$ test risk	0.178	0.009	12600 residualized prefixes
unseen rate $\rightarrow$ test risk	0.199	0.009	12600 residualized prefixes

Table 26: Controlled complexity diagnostics. Predictors and test risk are demeaned within dataset–budget–path groups before fitting a standardized one-variable regression. Positive estimates indicate that, even within the same dataset, calibration budget, and path rule, larger complexity pressure or unseen pattern rate is associated with higher test risk. This is diagnostic evidence, not a causal estimate.

Dataset	groups	mean within-group corr.	positive fraction
RewardBench	15	0.037	0.53
LLMBar	15	0.127	0.67
SummEval	18	0.484	1.00
Arena100K	12	0.331	1.00

Table 27: Within-dataset, within-budget, within-path correlations between  $H_K/n_M$  and test risk. Each group varies over splits and prefix sizes while holding the major confounders fixed.

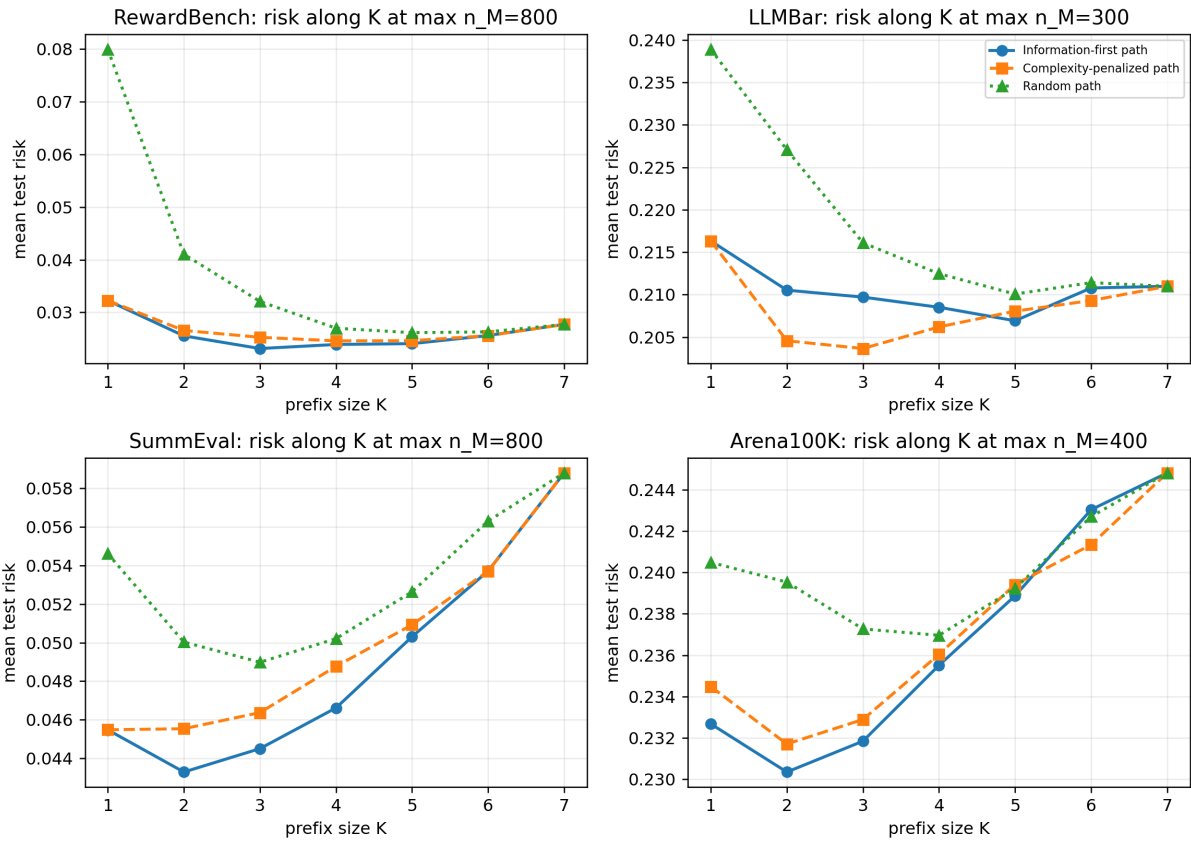


Figure 1: Joint-table finite-risk curves over prefix size  $K$  at the largest available calibration budget for each dataset.

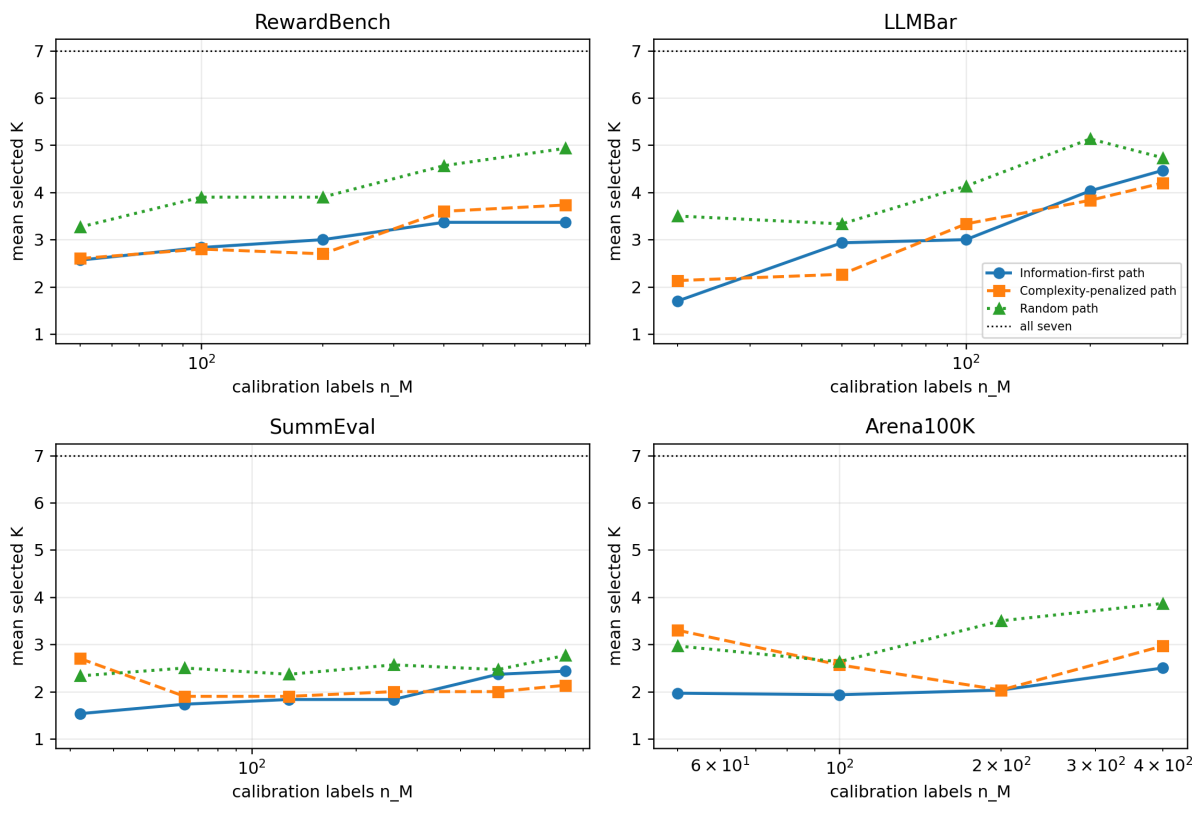


Figure 2: Selected joint-table prefix size as a function of calibration budget.

Strategy-separated finite-risk curves along  $K$

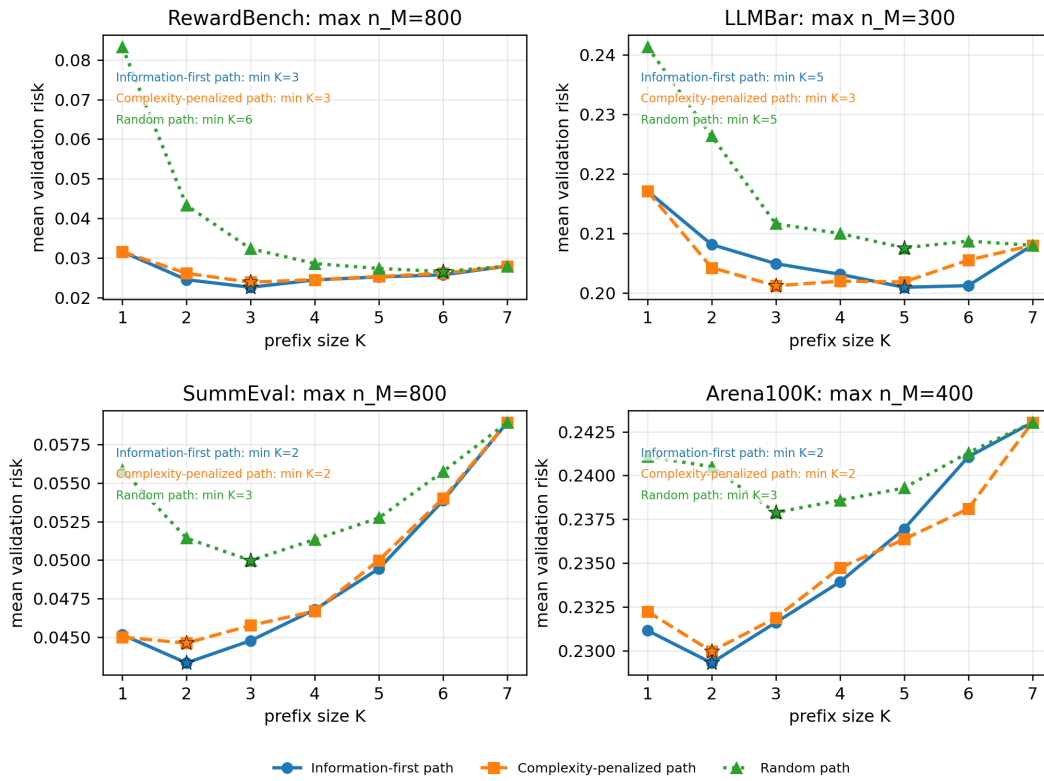


Figure 3: Strategy-separated joint-table validation-risk curves over prefix size  $K$ . Stars mark each path's mean validation-risk minimum.

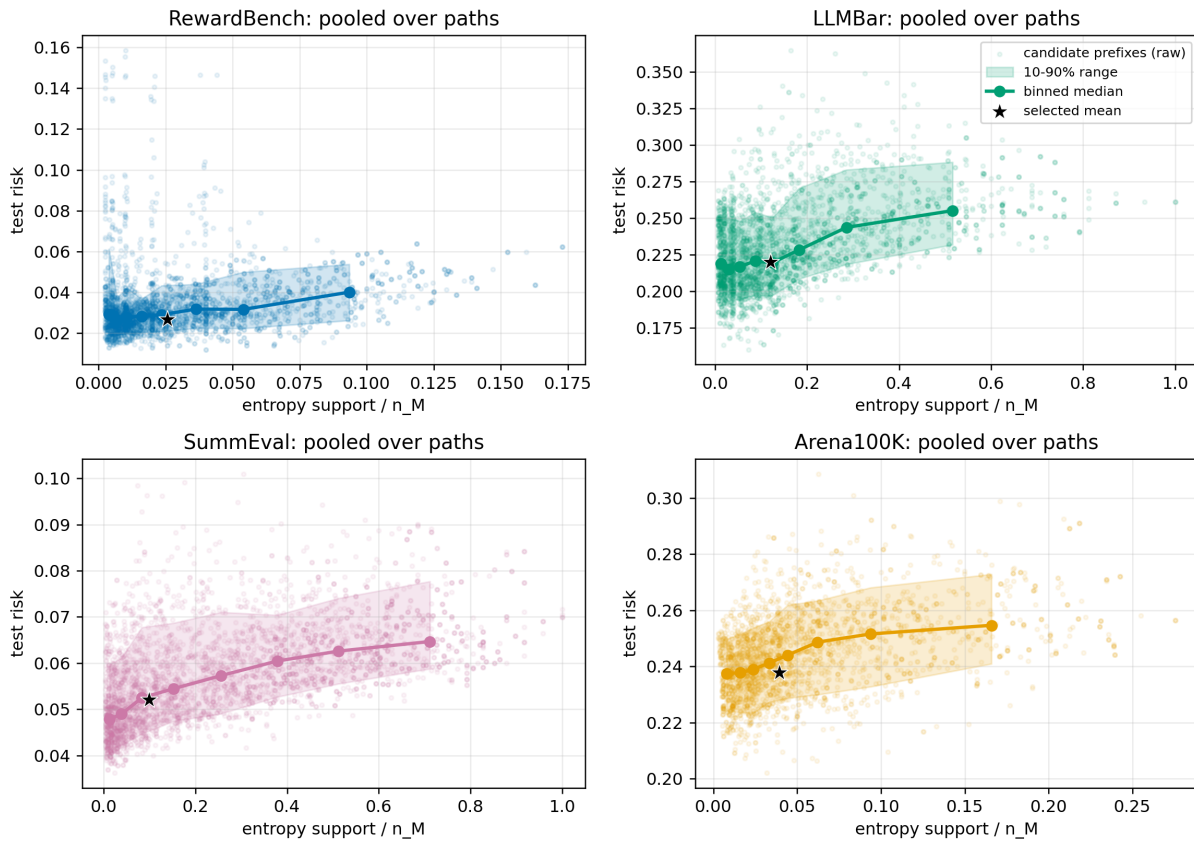


Figure 4: Joint-table finite risk versus the complexity proxy  $H_K/n_M$ , pooled over the three path rules.

Test risk increases in unseen-pattern regimes

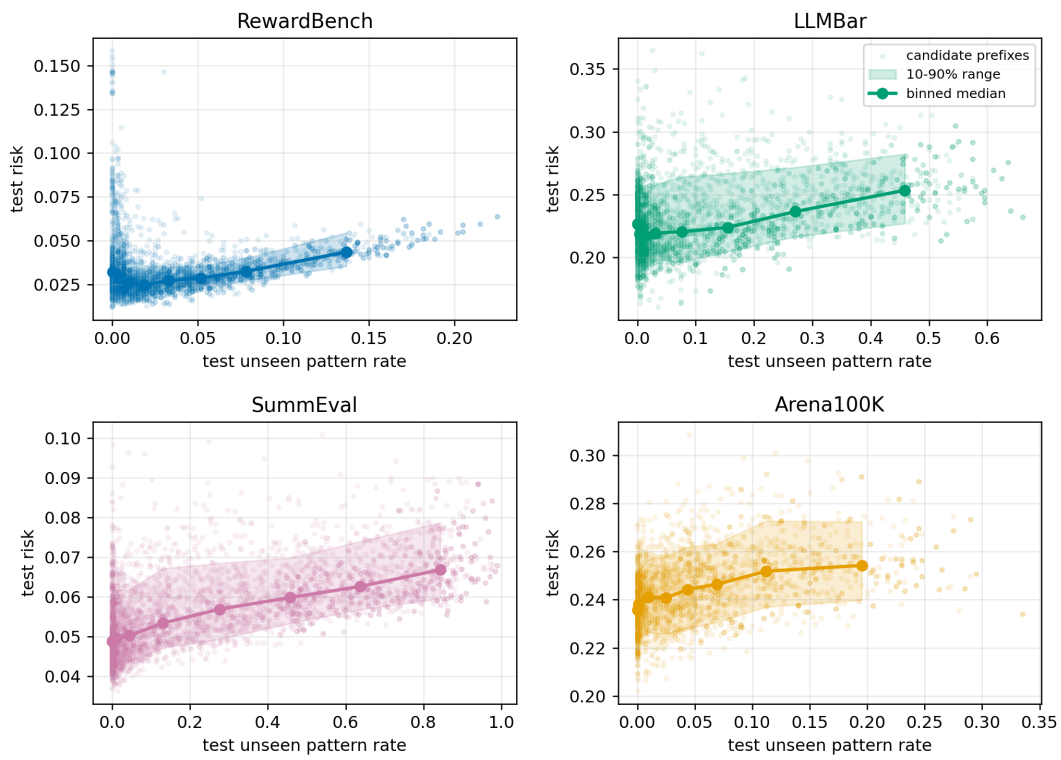


Figure 5: Joint-table test risk as a function of test-time unseen pattern rate.

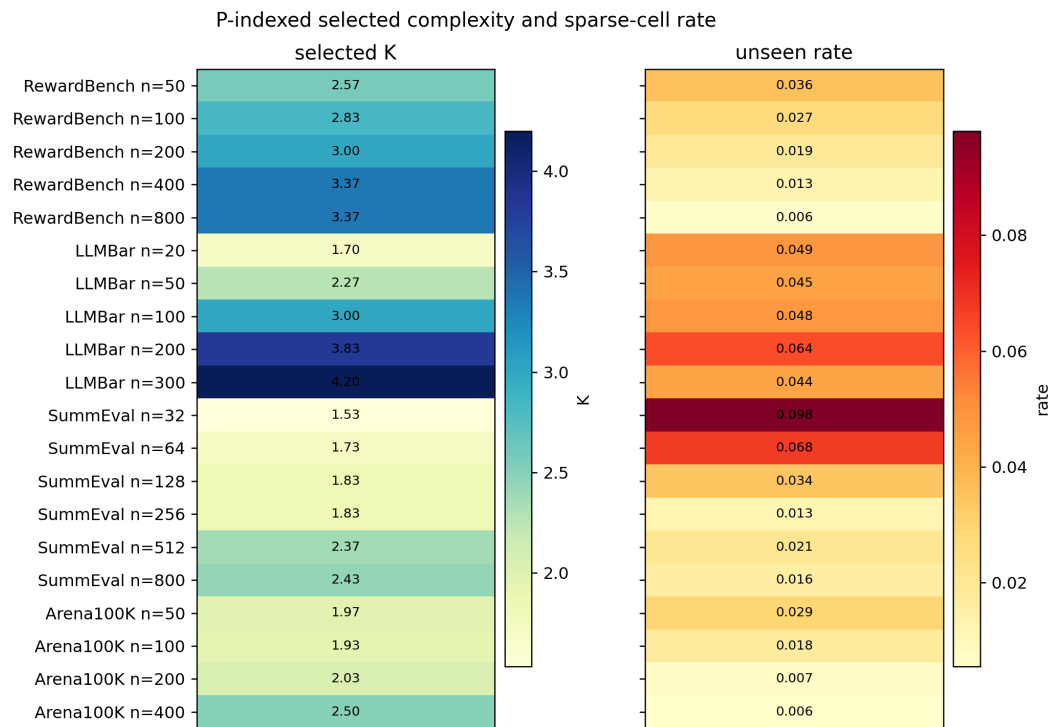


Figure 6: Distribution-indexed selected complexity and sparse-cell rate.

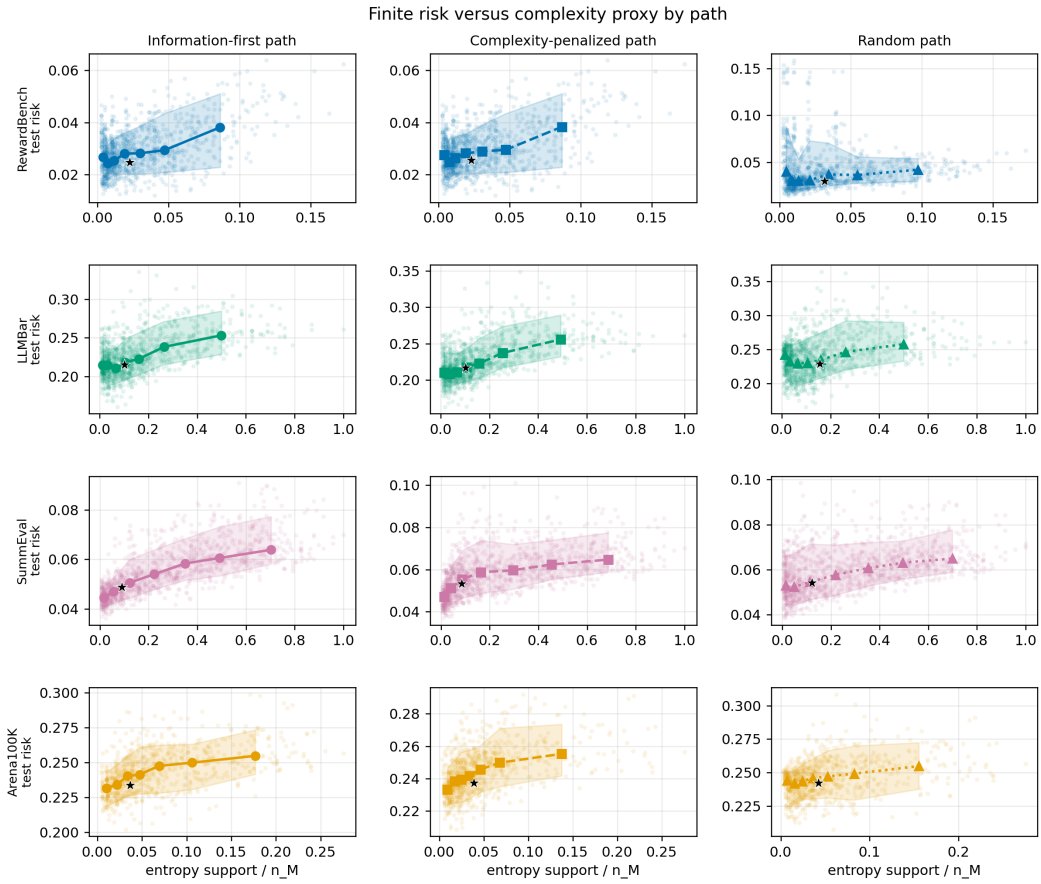


Figure 7: Path-separated version of Figure 4. Each row is a dataset and each column is a path rule. This diagnostic checks whether the pooled complexity-pressure pattern is solely an artifact of averaging information-first, complexity-penalized, and random paths.

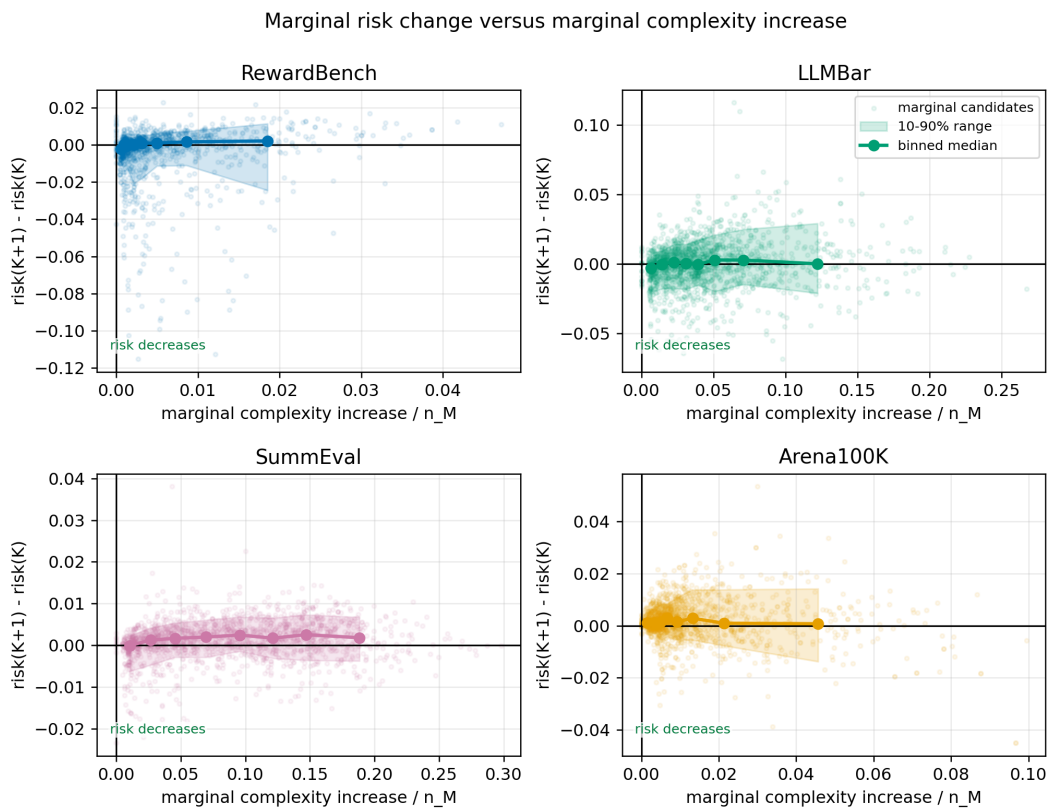


Figure 8: Marginal risk change versus marginal complexity increase when moving from  $K$  to  $K + 1$ . Values below zero indicate that adding the next judge reduces risk. The binned median and 10–90% band show that larger marginal complexity increases do not reliably produce risk reduction.

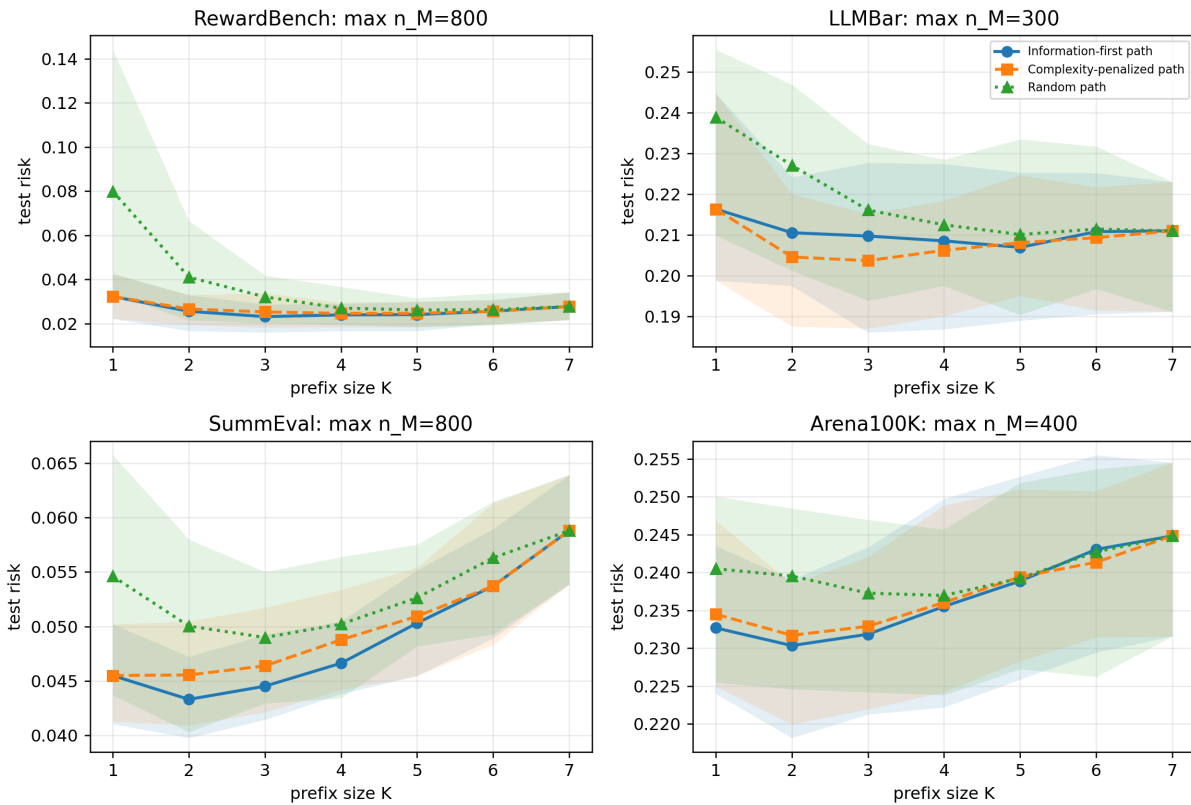


Figure 9: Uncertainty version of Figure 1. Lines show mean test risk over splits, and shaded bands show the 10–90% split range. This diagnostic checks whether the finite-risk non-monotonicity pattern is visible beyond a single average curve.

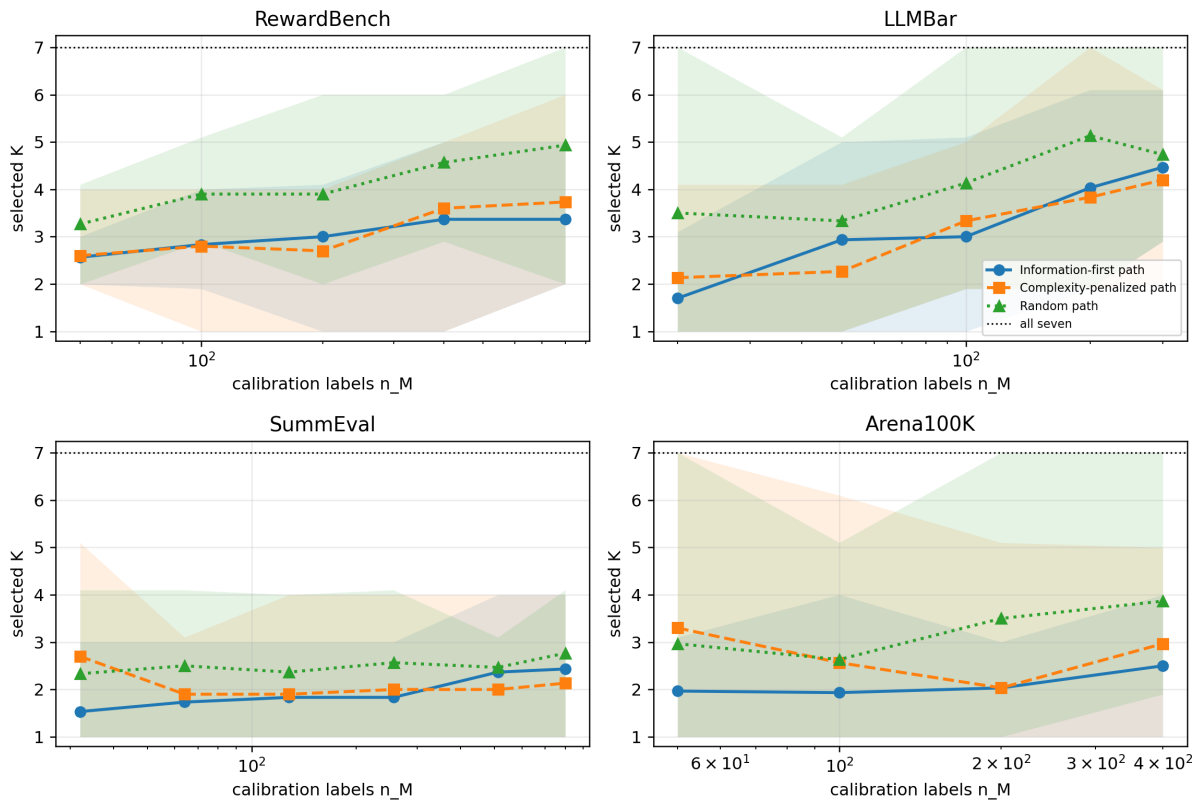


Figure 10: Uncertainty version of Figure 2. Lines show mean selected prefix size and shaded bands show the 10–90% split range. The plot makes explicit that selected complexity can be split-variable, especially when validation risks are close.